Article

SOURCE DATA | TRANSPARENT PROCESS

THE EMBO JOURNAL

Dysregulated miRNA biogenesis downstream of cellular stress and ALS-causing mutations: a new mechanism for ALS

Anna Emde[1], Chen Eitan[1], Lee-Loung Liou[2], Ryan T Libby[3], Natali Rivkin[1], Iddo Magen[1], Irit Reichenstein[1], Hagar Oppenheim[1], Raya Eilam[4], Aurelio Silvestroni[2], Betty Alajajian[2], Iddo Z Ben-Dov[5], Julianne Aebischer[6], Alon Savidor[7], Yishai Levin[7], Robert Sons[8], Scott M Hammond[8], John M Ravits[3,9,*], Thomas Möller[2,†] & Eran Hornstein[1,**,†]

Abstract

Interest in RNA dysfunction in amyotrophic lateral sclerosis (ALS) recently aroused upon discovering causative mutations in RNA-binding protein genes. Here, we show that extensive down-regulation of miRNA levels is a common molecular denominator for multiple forms of human ALS. We further demonstrate that pathogenic ALS-causing mutations are sufficient to inhibit miRNA biogenesis at the Dicing step. Abnormalities of the stress response are involved in the pathogenesis of neurodegeneration, including ALS. Accordingly, we describe a novel mechanism for modulating microRNA biogenesis under stress, involving stress granule formation and re-organization of DICER and AGO2 protein interactions with their partners. In line with this observation, enhancing DICER activity by a small molecule, enoxacin, is beneficial for neuromuscular function in two independent ALS mouse models. Characterizing miRNA biogenesis downstream of the stress response ties seemingly disparate pathways in neurodegeneration and further suggests that DICER and miRNAs affect neuronal integrity and are possible therapeutic targets.

Keywords microRNA, ALS, stress, neurodegeneration, DICER
Subject Categories Neuroscience; RNA Biology
DOI 10.15252/embj.201490493 | Received 9 November 2014 | Revised 5 July 2015 | Accepted 20 July 2015 | Published online 1 September 2015
The EMBO Journal (2015) 34: 2633–2651

See also: **S Bicker & G Schratt** (November 2015)

Introduction

Amyotrophic lateral sclerosis (ALS) is a neurodegenerative disease of the human motor neuron system. Mutations in genes encoding RNA-binding proteins were recently identified as causative in human ALS. These include TAR DNA-binding protein 43 (TDP-43) (Kabashi *et al*, 2008; Sreedharan *et al*, 2008; Liu-Yesucevitz *et al*, 2010; McDonald *et al*, 2011), fused in sarcoma (FUS) (Kwiatkowski *et al*, 2009; Vance *et al*, 2009; Bosco *et al*, 2010; Gal *et al*, 2010) and heterogeneous nuclear ribonucleoprotein A1 (hnRNPA1) (Kim *et al*, 2013).

Stress granules (SGs) are cytoplasmic sites for modulating mRNA translation and form in response to cellular stress (Anderson & Kedersha, 2008, 2009; Buchan & Parker, 2009). Intriguingly, among the RNA-binding proteins that are recruited into SGs, several are mutated in ALS or the related disorder fronto-temporal dementia (FTD), for example, TDP-43 and FUS.

Stress and SGs are thought to be involved in the pathogenesis of ALS, and SGs are observed in pathologic ALS/FTD specimen (Neumann *et al*, 2007; Volkening *et al*, 2009; Bosco *et al*, 2010; Dormann *et al*, 2010; Gal *et al*, 2010; Liu-Yesucevitz *et al*, 2010; Dewey *et al*, 2011; McDonald *et al*, 2011; Meyerowitz *et al*, 2011; Aulas *et al*, 2012; Baron *et al*, 2013; Daigle *et al*, 2013; Kim *et al*, 2013; Vance *et al*, 2013; reviewed in Dewey *et al*, 2012; Emde & Hornstein, 2014; Li *et al*, 2013b; Ling *et al*, 2013). SG formation is initiated by the phosphorylation of eukaryotic translation initiation factor 2 alpha (EIF2A) on serine-51 or by the expression of several aggregation-prone proteins that are capable of initiating SG

1 Department of Molecular Genetics, Weizmann Institute of Science, Rehovot, Israel
2 Department of Neurology, School of Medicine, University of Washington, Seattle, WA, USA
3 Translational Research Program, Benaroya Research Institute at Virginia Mason, Seattle, WA, USA
4 Veterinary Resources, Weizmann Institute of Science, Rehovot, Israel
5 Nephrology Department, Hadassah - Hebrew University Medical Center, Jerusalem, Israel
6 Brain Mind Institute, École Polytechnique Fédérale de Lausanne, Lausanne, Switzerland
7 de Botton Institute for Protein Profiling, The Nancy and Stephen Grand Israel National Center for Personalized Medicine, Weizmann Institute of Science, Rehovot, Israel
8 Department of Cell Biology and Physiology, School of Medicine, University of North Carolina, Chapel Hill, NC, USA
9 Department of Neurosciences, UC San Diego, La Jolla, CA, USA
*Corresponding author. Tel: +1 858 246 1154; E-mail: jravits@ucsd.edu
**Corresponding author. Tel: +972 89346215; Fax: +972 89344108; E-mail: eran.hornstein@weizmann.ac.il
†These authors share equal senior authorship [Correction added on 23 September 2015 after first online publication: due to a production error, in the version published online on 1 September 2015 the author affiliations and equal senior authorship were incorrectly noted. The correct listings are shown in this version.]

© 2015 The Authors

nucleation (Kedersha *et al*, 1999). Accordingly, modulation of EIF2A phosphorylation mitigates neurotoxicity in animal models of ALS (Saxena *et al*, 2009; Kim *et al*, 2014).

microRNAs (miRNAs) are small endogenous RNAs. Initial processing of primary miRNAs by Drosha/Dgcr8 (Gregory *et al*, 2004) yields an intermediate pre-miRNA that is further processed by the 500-kDa DICER multi-protein complex to form a mature miRNA. This complex contains DICER 1, ribonuclease type III (DICER) and its partners, Argonaute RISC catalytic component 2 (AGO2), TAR (HIV-1) RNA-binding protein 2 (also known as TRBP) and protein kinase, interferon-inducible double-stranded RNA-dependent activator (PACT) (Chendrimada *et al*, 2005; Haase *et al*, 2005; Lee *et al*, 2006). DICER activity is controlled by its core partners (Ma *et al*, 2008; Shan *et al*, 2008; Li *et al*, 2012; Lee *et al*, 2013) and the mature miRNA is loaded onto AGO2, creating a functional RNA-induced silencing complex (RISC).

DICER and its co-factors participate at multiple levels of the stress response (Emde & Hornstein, 2014). Thus, DICER contributes to stress resistance in selected tissues and its deficiency reduces stress tolerance (Mori *et al*, 2012). In addition, various stress-signaling cascades control AGO2 post-translational modifications, its translocation into SGs and its activity (Leung *et al*, 2006; Qi *et al*, 2008; Zeng *et al*, 2008; Shen *et al*, 2013).

We previously demonstrated that loss of miRNA biogenesis is sufficient to cause spinal motor neuron degeneration *in vivo* (Haramati *et al*, 2010). In the current work, we demonstrate that reduction in miRNA levels is a common molecular denominator for multiple forms of familial and sporadic human ALS and that enhancement of DICER activity is beneficial *in vivo* in two independent ALS mouse models. The observations establish a novel pathway downstream of the stress response that controls DICER complex activity. The regulation of DICER involves stress granule assembly and dynamic interactions with SG proteins. This new mechanism for the control of miRNA biogenesis offers novel therapeutic targets for ALS.

Results

miRNAs are down-regulated in motor neurons of human ALS patients

We recently demonstrated that conditional inactivation of DICER in motor neurons is sufficient to cause spinal motor neuron degeneration *in vivo* (Haramati *et al*, 2010). Additional works from other groups further suggest the involvement of miRNAs in ALS pathogenesis (Williams *et al*, 2009; Buratti *et al*, 2010; Kawahara & Mieda-Sato, 2012; Morlando *et al*, 2012; Droppelmann *et al*, 2013; Freischmidt *et al*, 2013; Koval *et al*, 2013; Zhang *et al*, 2013). To pursue this, we examined miRNA expression in lumbar motor neurons of sporadic ALS (sALS) spinal cords isolated by laser capture microdissection (LCM). Global down-regulation of miRNAs was observed in motor neurons. The observation seemed specific to motor neurons since RNA extracted from surrounding, motor neuron-depleted ventral-horn tissue of sALS patients or from neurons of Clarke's column (non-motor neuron) isolated by LCM within the same nervous systems did not exhibit such global changes in miRNA expression (Fig 1A–C). The observations of miRNA down-regulation were substantiated by miRNA *in situ* hybridization, which revealed down-regulation of miR-9 and miR-124 in patient tissue, relative to control tissue and to the hybridization signal of U6 RNA (Fig 1D). We next investigated whether miRNAs display a similar profile in fALS cases. Indeed, analyzing two nervous systems carrying familial SOD1 A4V mutation, revealed similar down-regulation of miRNAs (Fig 1E and F) that correlated with miRNA changes, observed in sALS (Pearson's correlation coefficient = 0.3). Our data suggest that changes in miRNA expression, which were previously reported in ALS spinal cord extracts (Campos-Melo *et al*, 2013), are primarily due to changes in miRNA expression in motor neurons. Attempts to measure pre-miRNAs in human LCM samples were unsuccessful, probably due to the low abundance of these intermediate precursors. Noteworthy, expression and splicing data for changes in mRNAs encoding miRNA biogenesis factors from the relevant ALS patients did not reveal any change, relative to controls (Rabin *et al*, 2009). Additionally, 27 long ncRNAs tested were similarly expressed in another cohort of 12 non-ALS and 12 sporadic ALS nervous systems, with Pearson's correlation of 0.9882. Since miRNAs are globally down-regulated in sALS cases that are genetically unrelated, reduced miRNA expression in motor neurons appears to be a common denominator of various forms of ALS.

Cellular stress affects pre-miRNA processing

Stress pathways are thought to control miRNA activity (Leung & Sharp, 2010; Mendell & Olson, 2012; Emde & Hornstein, 2014), but the idea that cellular stress might broadly regulate miRNA biogenesis has not been tested. We sought to do so by the measurement of the relative levels of mature miRNAs and pre-miRNAs under several stress conditions. We further defined an "inhibition score" that approximates a value of one, when DICER processes pre-miRNAs effectively, as in wild-type conditions, and increases >1, when miRNA biogenesis is inhibited, relative to control (Fig 2A).

We chose representative miRNAs that are expressed in human and mouse motor neurons including miR-10b, miR-30a and miR-103 (abundantly expressed in isolated mouse motor neurons); miR-218, miR-30c, miR-138 and let-7b (highly expressed in human motor neurons); miR-132, let-7c and let-7d (neuronal, mid-range in human); and miR-143 and let-7a (low expression in human neurons).

We triggered cellular stress in the hybrid motor neuron cell line NSC-34; using thapsigargin induced markers of ER stress (Appendix Fig S1A), down-regulated mature miRNA levels and up-regulated pre-miRNA levels, relative to control, demonstrating the inhibition of miRNA biogenesis (Fig 2B–D). In addition, application of oxidative stressors, paraquat or sodium arsenite, led to the inhibition of miRNA biogenesis (Fig 2E–J, Appendix Fig S1B).

To test whether changes in DICER or its co-factors are down-regulated as a result of stress, we measured protein levels by Western blot analysis. The expression levels of the four DICER complex proteins were not down-regulated by two independent stressors (thapsigargin, paraquat). DICER and AGO2 levels were not reduced by sodium arsenite as well, but PACT and TRBP levels were reduced by 1/3 (Appendix Fig S2 related to Fig 2). We conclude that alteration of DICER activity may occur even without reduction in DICER complex components.

 © 2015 The Authors

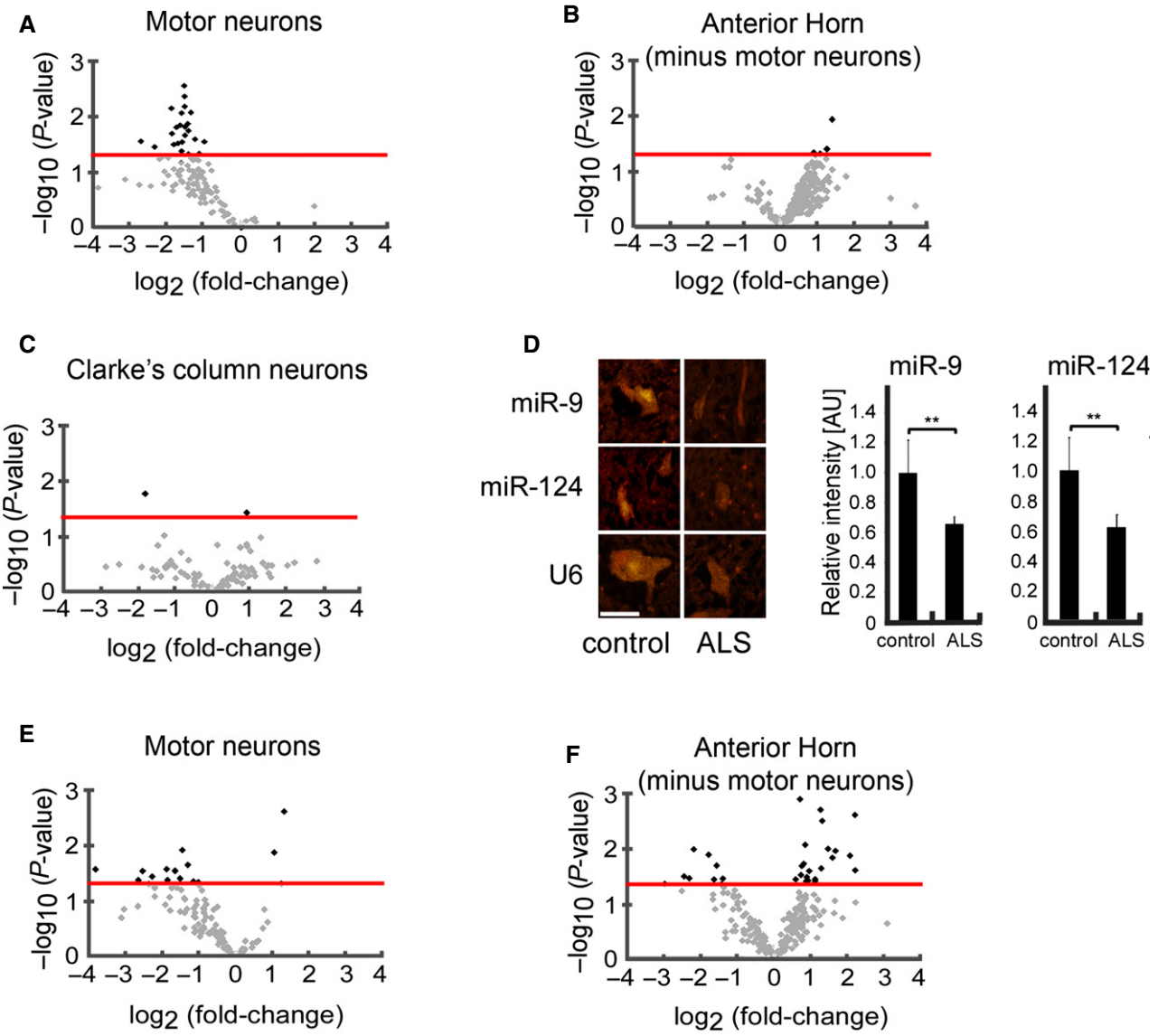

Figure 1. miRNAs are down-regulated in human ALS motor neurons.

A–C Volcano plots of *P*-values (*y*-axis $\log_{10}$ scale) for relative miRNA expression (*x*-axis $\log_2$ scale). (A) Human lumbar motor neurons (eight sporadic ALS nervous systems, nine non-neurodegeneration controls), (B) anterior horn tissue without motor neurons from the same individuals (10 sporadic ALS nervous systems, nine controls) and (C) miRNA expression in Clarke's column (three sporadic ALS nervous systems versus three controls).

D Representative micrographs with *in situ* hybridization for miR-9 and miR-124; scale bar indicates 10 μM. Bar graph displays signal intensity, quantified in 300 different motor neurons of two ALS nervous systems and two controls, normalized to U6 *in situ* hybridization signal. Error bars represent s.d.

E, F miRNA expression in lumbar motor neurons of two familial ALS nervous systems versus nine controls (E) and the respective anterior horn tissue depleted of motor neurons (F). Analyses were performed as in (A–C).

Data information: (A–C, E, F) Black dots indicate $P < 0.05$; light gray dots are non-significant. miRNAs were measured using TaqMan array microRNA cards, normalized to the average of three control RNAs: RNU48/SNORD48, RNU44/SNORD44 and U6 and subjected to ANOVA Statistics (DataAssist, Life Technologies). Source data are available online for this figure.

Expression of ALS-causing genes inhibits pre-miRNA processing

To assess whether ALS-causing genes affect miRNA biogenesis similar to chemical stressors, we transfected NSC-34 cells with vectors of wild-type FUS, TDP-43 and SOD1 or mutant forms of the same genes, specifically FUS R495X (Bosco *et al*, 2010; Waibel *et al*, 2010), TDP-43 A315T (Gitcho *et al*, 2008) and SOD1 G93A (Rosen *et al*, 1993) (Fig 3A). We observed inhibition in biogenesis of many of the miRNA species tested, relative to the corresponding control sample values, after overexpression of wild-type or mutant FUS and TDP-43 (Fig 3B–E, Appendix Fig S3). The inhibitory effect of wild-type SOD1 or G93A mutant on miRNA biogenesis was consistent with this, but more limited (Fig 3F and G). The deleterious effect of higher-than-normal levels of

© 2015 The Authors

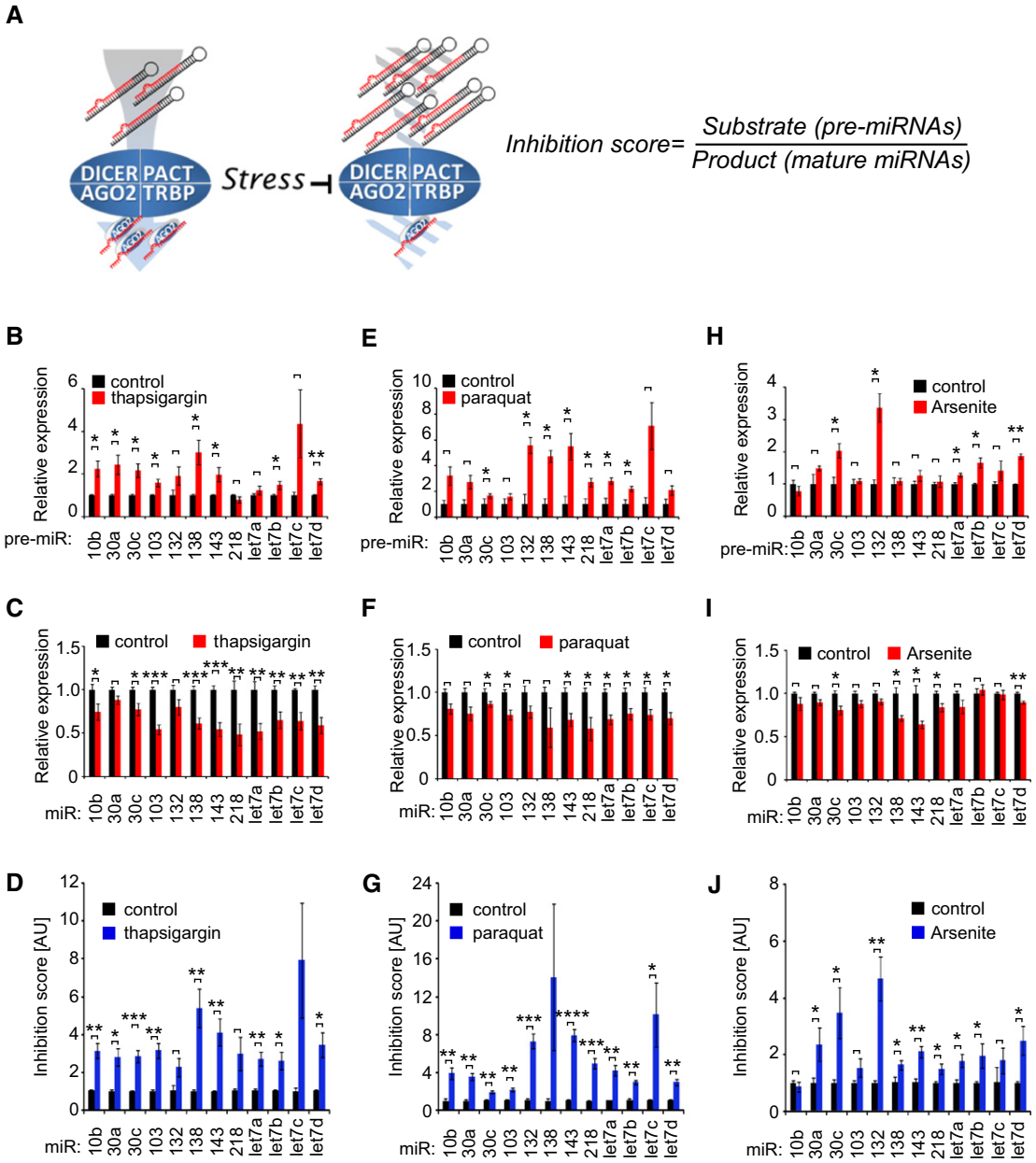

Figure 2. Different cellular stressors lead to impaired miRNA biogenesis.

A Diagram depicting the working hypothesis. The DICER complex is composed of DICER, AGO2, PACT and TRBP, and the catalysis of pre-miRNA hairpins into mature AGO2-loaded miRNAs is schematically presented by a vertical arrow. Stress inhibits Dicing, resulting in the accumulation of substrate (pre-miRNA) and reduction in product levels (mature miRNA). The ratio of substrate to product, defined as "inhibition score," approximates a value of 1 in the unmanipulated wild-type conditions. Inhibition score values greater than 1, reflect reduced DICER activity.

B–J Pre-miRNA (B, E, H) and miRNA (C, F, I) expression analysis and their corresponding inhibition score (D, G, J). NSC-34 cells treated with thapsigargin (10 nM for 24 h) or control carrier (DMSO) (B–D), paraquat (25 μM for 24 h) or control carrier (water) (E–G) and sodium arsenite (0.5 mM for 60 min) or control carrier (water) (H–J). Displayed are average and standard error of the mean (s.e.m.) for qPCR analyses of at least three independent experiments, normalized to the expression levels in control treatments. Pre-miRNA levels were normalized to beta-actin and Gapdh, and miRNAs were normalized to Snord68 and Snord70. *P*-values of qPCR were calculated via ANOVA statistics with DataAssist, and with two-sided Student's *t*-test for inhibition score. Significant *P*-values are indicated by $*P < 0.05$, $**P < 0.01$, $***P < 0.001$, $****P < 0.0001$.

Source data are available online for this figure.

wild-type FUS, TDP-43 or SOD1 is in accordance with the previous reports (Jaarsma *et al*, 2000; Wils *et al*, 2010; Igaz *et al*, 2011; Mitchell *et al*, 2013). Western blot analysis revealed that the levels of DICER, AGO2, PACT and TRBP did not change by the overexpression of wild-type, or mutant forms of FUS (Appendix Fig S4 related to Fig 3).

 © 2015 The Authors

In order to test DICER activity directly, we devised a cell-free Dicing assay, using cell lysates and synthetic double-stranded RNA, carrying a quencher on a 25-nt passenger strand and a CY3 fluorophore conjugate on a 27-nt precursor guide strand. Dicing activity enables the dissociation of a fluorophore conjugate RNA from the quencher and fluorescence (Fig 4A). The assay demonstrated reduction in DICER catalytic activity in lysates of cells treated with sodium arsenite, paraquat or thapsigargin (Fig 4B and C). Importantly, overexpression of ALS-causing mutants or their respective wild-type forms also reduced DICER activity (Fig 4D). Noteworthy is that the *in vitro* assay probably provides an underestimate of the changes in DICER activity, due to the extensive dilution of soluble

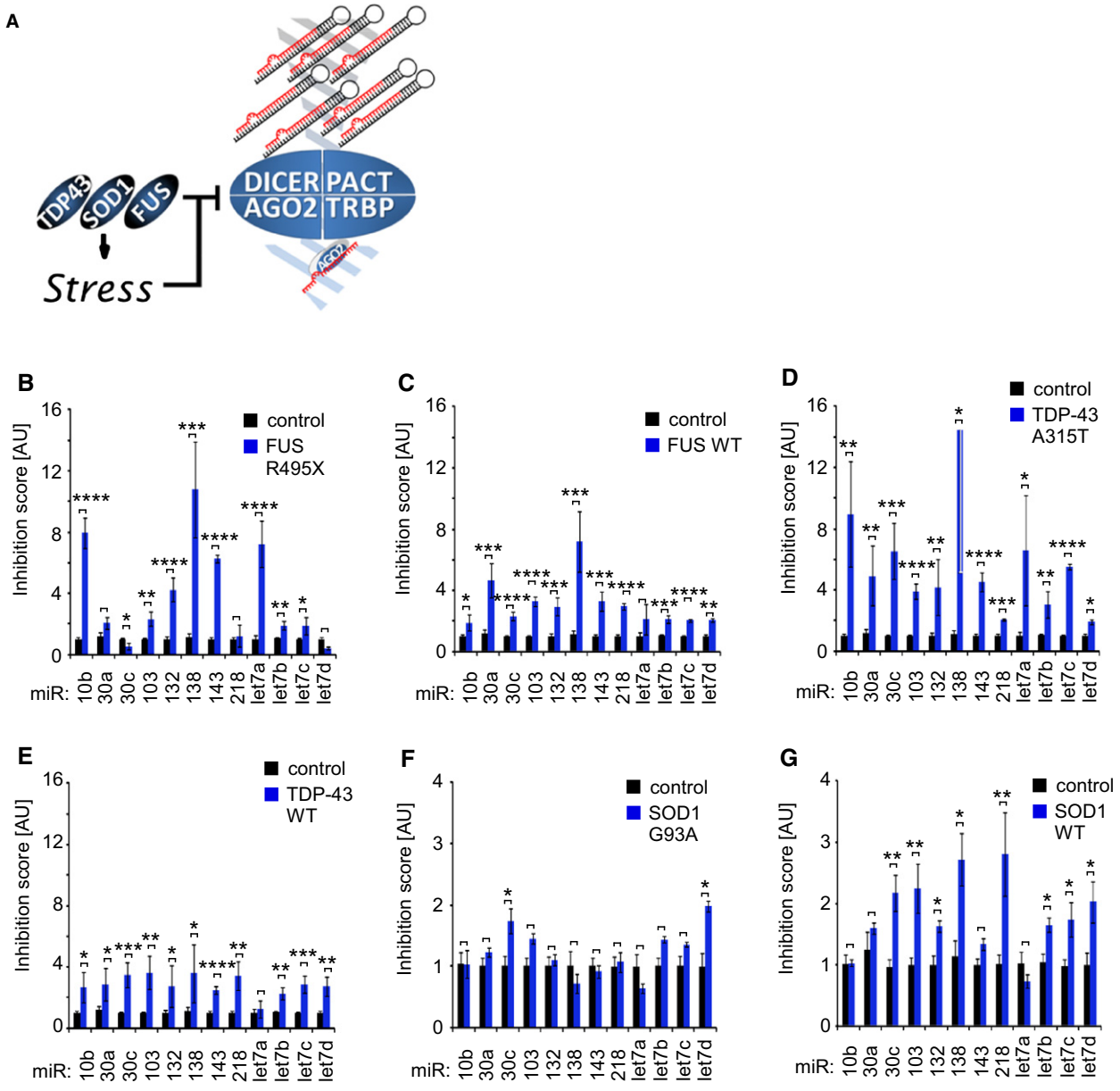

Figure 3. Over-expression of ALS-causing mutant proteins leads to impaired miRNA biogenesis.

A Diagram depicting the working hypothesis that expression of ALS-causing TDP-43, FUS or SOD1 attenuates DICER complex activity directly, or through induction of stress.

B–G Inhibition score of FUS R495X (B), wild-type FUS (C), TDP-43 A315T (D), wild-type TDP-43 (E), SOD1 G93A (F) or wild-type SOD1 (G). The calculated values are based on qPCR analysis results of pre-miRNAs, mature miRNAs of NSC-34 cell RNA, 72 h post-transfection, which is presented in Appendix Fig S3. The inhibition score of individual pre-miRNA:miRNA pairs was normalized to values in cells transfected with control vector. Shown are average and s.e.m. of > 3 independent experiments, except for pre-miRNAs in the study of FUS R495X ($n = 2$). *P*-values were calculated by two-sided Student's *t*-test, $^{*}P < 0.05$, $^{**}P < 0.01$, $^{***}P < 0.001$, $^{****}P < 0.0001$.

Source data are available online for this figure.

© 2015 The Authors

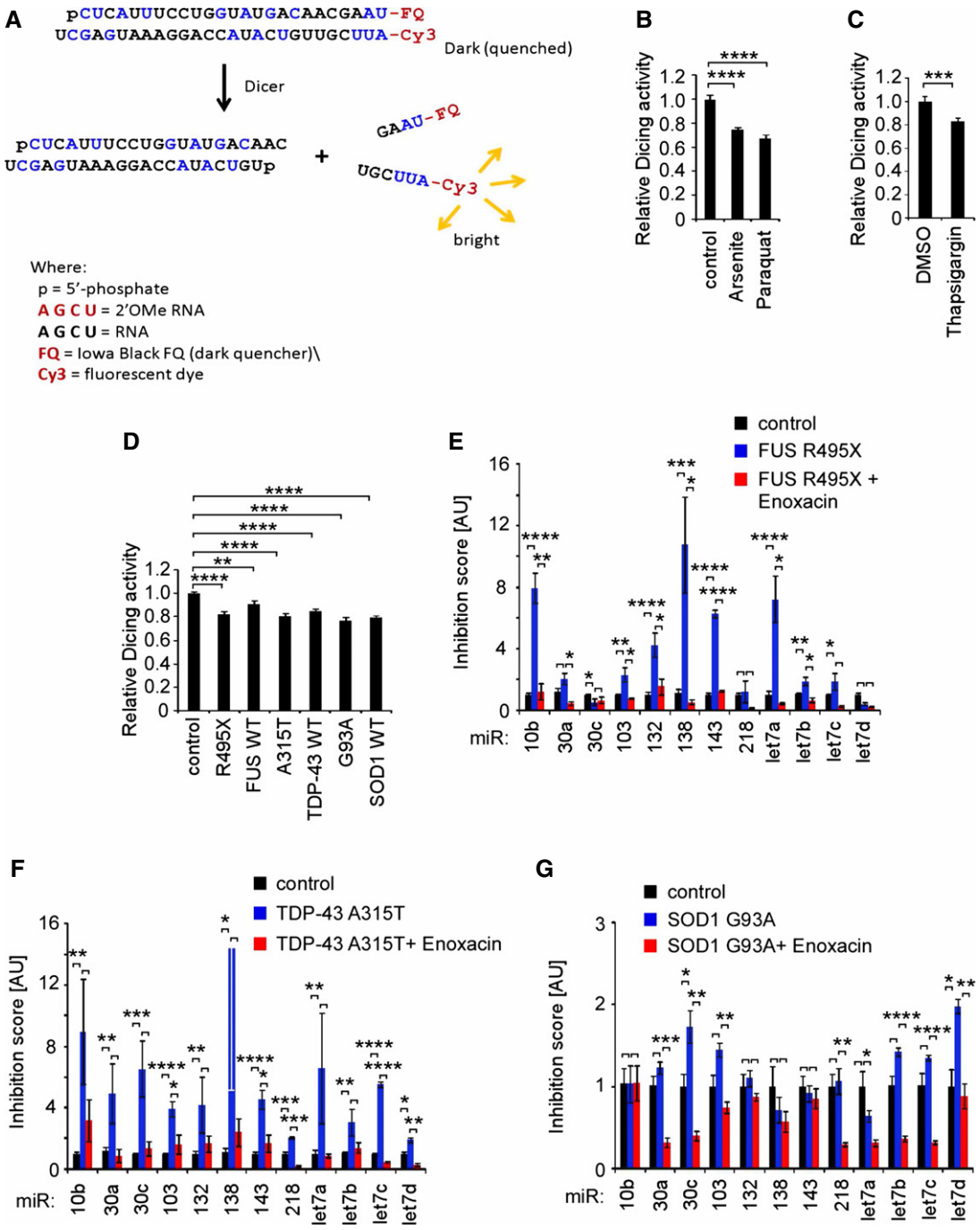

Figure 4. Stress or over-expression of ALS-causing mutants inhibits DICER activity in cell lysates.

A Diagram of the *in vitro* DICER activity assay, in which an annealed double-stranded RNA substrate is composed of a fluorophore-conjugated 27-nt guide strand and a 25-nt passenger strand conjugated to a quencher moiety. The DICER complex releases a 21-nt mature single-stranded guide RNA, whose fluorescence correlates with DICER activity.

B, C Dicing *in vitro* assay was performed in NSC-34 lysates after treatment with (B) sodium arsenite (0.5 mM for 60 min), paraquat (25 μM for 24 h) or control carrier (water), or alternatively (C) with thapsigargin (10 nM for 24 h) versus control carrier DMSO.

D Dicing *in vitro* assay was performed in HEK293 cell extracts 72 h post-transfection with the indicated plasmids.

E–G Inhibition score of DICER activity in cells transfected with ALS-causing mutants FUS R495X (E), TDP-43 A315T (F) or SOD1 G93A (G) and treated with carrier (buffer) or enoxacin (100 μM) for 72 h. The calculated values are based on qPCR analysis of pre-miRNAs, and mature miRNAs of NSC-34 cell RNA that is presented in Appendix Fig S5. Inhibition score of individual pre-miRNA:miRNA pairs was normalized to values in cells transfected with control vector.

Data information: (B–G) Shown are average and s.e.m. of > 3 independent experiments. *P*-values were calculated by two-sided Student's *t*-test, $*P < 0.05$, $**P < 0.01$, $***P < 0.001$, $****P < 0.0001$.

Source data are available online for this figure.

© 2015 The Authors

DICER cofactors in the reaction buffers. Therefore, overexpression of ALS genes, mutation in ALS genes and the application of oxidative or ER stress all inhibit DICER catalytic activity.

Enoxacin ameliorates ALS-induced defects in pre-miRNA processing

Next, we hypothesized that enhancing Dicing complex activity might reverse the negative effect of the ALS-causing mutant proteins on miRNA processing. We tested this hypothesis by employing enoxacin, a fluoroquinolone antibiotic that is commonly used for the treatment of urinary tract and airway infections. Enoxacin is known to increase miRNA biogenesis via increasing the binding affinity of TRBP and pre-miRNAs (Shan *et al*, 2008; Melo *et al*, 2011). Intriguingly, the impairments in pre-miRNA processing that were evident in NSC-34 cells upon transfection with vectors expressing ALS-causing mutants FUS R495X, TDP-43 A315T or SOD1 G93A were partially ameliorated by applying enoxacin (100 μM for 72 h) to transfected cultures (Fig 4E–G and Appendix Fig S5). Therefore, enoxacin studies further support the view that DICER activity is impaired in culture models of ALS.

Stress granule formation controls miRNA biogenesis

To gain further mechanistic insight, we performed targeted mass spectrometry analysis of AGO2 and DICER protein interactions under cellular stress (Fig 5A). We examined a set of proteins that were co-immunoprecipitated with either AGO2 or DICER in a preliminary unbiased screen. Targeted mass spectrometry revealed enhanced interactions of AGO2 with DICER in cells that were treated with sodium arsenite, relative to basal conditions (Fig 5B and C). We report increased AGO2 binding to DICER, which was previously shown to decrease DICER complex activity (Tahbaz *et al*, 2004).

As DICER complex composition controls miRNA biogenesis (Lee & Doudna, 2012; Lee *et al*, 2013), we measured additional AGO2 and DICER interactions. HSP90 and co-chaperone p23, which regulate the interactions of DICER with AGO2 (Tahbaz *et al*, 2004; Pare *et al*, 2013), increased their interactions with DICER under stress (Fig 5B). These interactions potentially stabilize an intermediate DICER–AGO2–P23–HSP90 complex (Pare *et al*, 2013), thereby inhibiting DICER catalytic activity. In addition, cellular stress increased AGO2 and/or DICER protein interactions with SG components EIF2A, EIF3 (Kedersha *et al*, 2005) and EIF5A (Li *et al*, 2010) and with poly(rC)-binding proteins PCBP1 (hnRNP E1) and PCBP2 (hnRNP E2) (Li *et al*, 2012) (Fig 5B and C). PCBPs are iron chaperones (Shi *et al*, 2008; Nandal *et al*, 2011), found in SGs and P-bodies (Fujimura *et al*, 2008, 2009). PCBP2 binds to miRNA precursors and presents them to DICER for efficient processing (Li *et al*, 2012). Therefore, the binding of PCBP1 and 2 to AGO2 and DICER exposes an additional layer of complexity in the regulation of miRNA biogenesis under stress.

Finally, AGO2 is phosphorylated by the p38 mitogen-activated protein kinase on serine-378 under stress (Zeng *et al*, 2008), consistent with a > 10-fold increase in AGO2 serine-387 phosphorylation in our system (Fig 5C). Intriguingly, p38 was reported to be persistently activated in ALS (Tortarolo *et al*, 2003). We further validated increased interactions of AGO2 with PCBP1, by AGO2 immunoprecipitation and Western blot analysis. DICER pull-down was marginally significant, and we could not validate the increased interaction of PACT with AGO2 (Fig 5D).

Taken together, these observations point toward substantial changes in the interactions of DICER and AGO2 with SG components. Next, we tested the hypothesis that SG formation may be sufficient to attenuate DICER complex activity. We overexpressed TIAR, a known initiator of stress granule formation (Kedersha *et al*, 1999), which reduced DICER catalytic activity in a cell-free assay (Fig 5E). EIF5A is a translation elongation factor, which is engaged with SGs under stress (Li *et al*, 2010) and also with DICER (Fig 5B). We demonstrated that EIF5A overexpression reduced DICER catalytic activity in a cell-free assay and in cells (Fig 5E and F and Appendix Fig S6A and B).

Several cellular stress-signaling cascades converge into the phosphorylation of Serine-51 of the translation initiation factor 2 alpha (EIF2A), thereby driving SG formation (Hinnebusch, 2005; Kedersha *et al*, 2005). Because EIF2A interactions with AGO2 and/or DICER increased by stress (Fig 5B and C), we tested the implications of overexpressing a phosphomimetic version of EIF2A (S51D). Expression of EIF2A S51D resulted in inhibition of DICER activity (Fig 5G and Appendix Fig S6C and D), further linking stress signaling to reduced miRNA biogenesis. Accordingly, phosphorylation-resistant serine-to-alanine-mutated EIF2A (S51A) (Costa-Mattioli *et al*, 2007) enabled a partial recovery from thapsigargin-induced attenuation of DICER complex activity in mouse embryonic fibroblasts (Appendix Fig S7 related to Fig 5).

To test whether the experimental manipulations we used are sufficient to induce visible SGs, we utilized immunofluorescence microscopy. This study revealed the onset of TIA1-positive stress granules with a set of chemical SG inducers, or after transient transfection with vectors expressing wild-type or mutant forms of FUS, TDP-43 or SOD1. It may be that high plasmid copy number and the stress of the transient transfection contributed to the induction of SGs by wild-type FUS, which was not reported in a stably transfected cell line (Bosco *et al*, 2010; Dormann *et al*, 2010; Daigle *et al*, 2013).

In addition, overexpression of SG proteins that were sufficient to inhibit DICER activity, EIF5A, EIF2A S51D or TIAR led to the formation of TIA1-positive SGs (Fig 6). Intriguingly, under all these conditions, AGO2 was co-localized with TIA1 in SGs, in accordance with the previous reports that observed AGO2 recruitment into SGs (Leung *et al*, 2006; Wu *et al*, 2011). Therefore, interactions of SG proteins with AGO2 and/or DICER directly contribute to the attenuation of DICER activity.

We next tested the effect of SGs on DICER activity via chemical induction or blockade of SG formation (Fig 7A). NSC-34 cells were treated with puromycin (1 μg/ml, 24 h), which drives dismantling of translating polysomes, thereby inducing SGs (Blobel & Sabatini, 1971). Puromycin decreased the efficacy of miRNA biogenesis in a cell-free Dicing assay (Fig 7B) and in cells, as measured by qPCR (Fig 7C and Appendix Fig S8A and B). Notably, puromycin (1 μg/ml, 24 h) reduced DICER and TRBP levels by 44 and 31%, respectively (Appendix Fig S9A and B related to Fig 7). Because the interpretation of the puromycin experiment can take into consideration reduction in DICER/TRBP levels, we sought a complementary approach to test whether inhibition of SG formation recovers miRNA biogenesis from ALS mutant-induced Dicing defects. Cycloheximide (CHX) is known to dissolve pre-formed SGs (Kedersha *et al*, 2000). The application of CHX to cultures transfected with

© 2015 The Authors

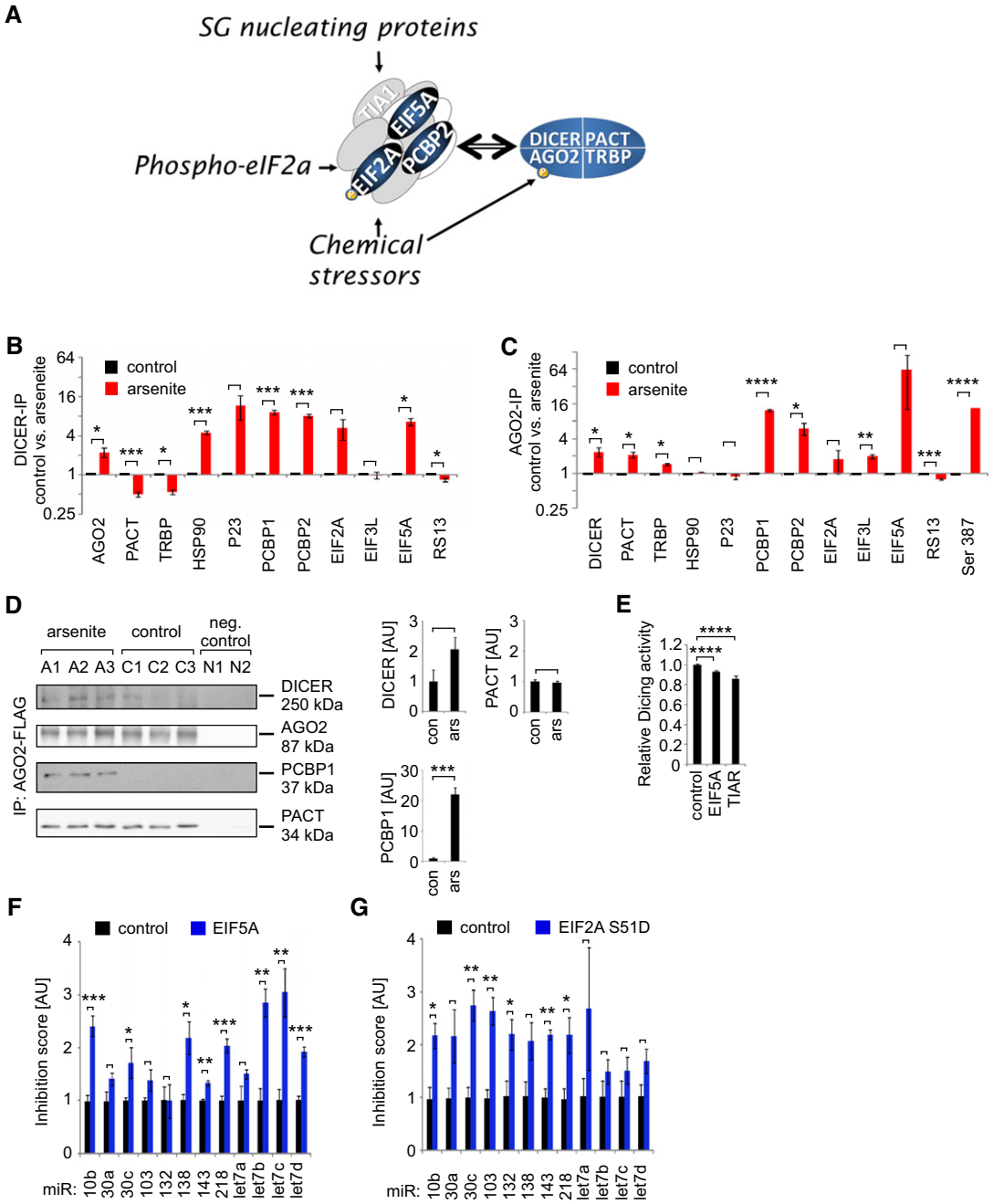

Figure 5. Stress granule proteins interact with DICER complex components and modulate Dicing activity.

A Diagram depicting the working hypothesis that DICER complex interactions with stress granule proteins is modified by chemical stressors, overexpression of phosphomimetic EIF2A or overexpression of stress granule proteins.

B, C Targeted mass spectrometry analysis of proteins, co-immunoprecipitated with DICER-FLAG (B) or AGO2-FLAG (C), from HEK293 cells treated with sodium arsenite (0.5 mM, 60 min). Data are presented as ratio of averaged peptide counts from three different peptide standards per protein, relative to peptide levels in untreated cells. Note that two peptides were identified above threshold for EIF5A and for TRBP in the AGO2-IP, and AGO2 phospho-S387 is measured by a single peptide. Averages ± s.e.m.; $*P < 0.05$, $**P < 0.01$, $***P < 0.001$, $****P < 0.0001$ by two-sided Student's *t*-test, between arsenite and control treatment are denoted.

D Western blot study and densitometry of DICER, AGO2, PCBP1 and PACT after AGO2-FLAG immunoprecipitation, in three different biological replicates without or with sodium arsenite (0.5 mM, 60 min). Averages ± s.e.m.; two-sided Student's *t*-test, $***P < 0.001$, for changes in AGO2 co-immunoprecipitated protein levels.

E *In vitro* Dicing activity assay in HEK293 cell lysate 72 h post-transfection with EIF5A or TIAR. Averages ± s.e.m.; $****P < 0.0001$ by two-sided Student's *t*-test from > 3 independent biological replicates.

F, G Inhibition score of individual pre-miRNA:miRNA pairs of HEK293 cells transfected with EIF5A (F) or phosphomimetic form of EIF2A (S51D) (G). Calculated values are based on qPCR analysis of pre-miRNAs and mature miRNAs of NSC-34 cell RNA, presented in Appendix Fig S6. Inhibition score was normalized to values in cells transfected with control vector. Averages ± s.e.m.; $*P < 0.05$, $**P < 0.01$, $***P < 0.001$ by two-sided Student's *t*-test from > 3 independent biological replicates.

Source data are available online for this figure.

© 2015 The Authors

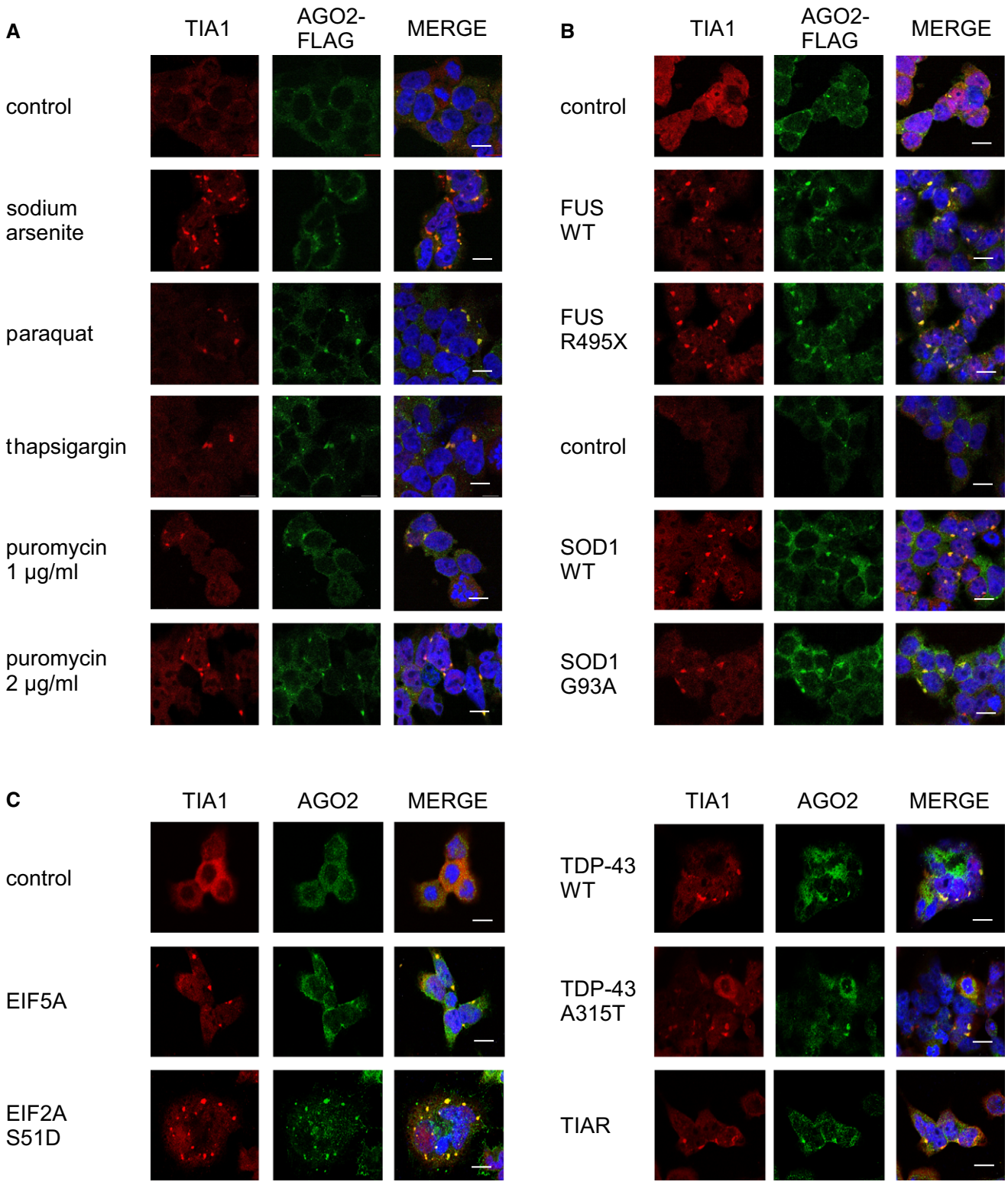

Figure 6. Localization of AGO2 to TIA1-positive stress granules.

A AGO2-FLAG HEK293 cells were treated with sodium arsenite (0.5 mM, 60 min), paraquat (25 µM, 24 h) or carrier (water), thapsigargin (10 nM, 24 h) or DMSO, puromycin (1 µg/ml and 2 µg/ml for 24 h) or carrier (water).

B Depicted are micrographs of AGO2-FLAG HEK293 cells transfected with plasmids as indicated and stained with antibodies for FLAG and TIA1, 72 h post-transfection.

C Micrographs of HEK293 cells transfected with plasmids as indicated and stained with antibodies for AGO2 and TIA1, 72 h post-transfection.

Data information: Scale bars indicate 10 µm.

© 2015 The Authors

FUS R495X-, TDP-43 A315T- or SOD1 G93A-expressing vectors was able to mitigate the reduction in DICER complex activity (Fig 7D–F and Appendix Fig S8C–H) and reduced the abundance of visible SG that were quantified by confocal microscopy (Fig 7G and H). Noteworthy, it is unlikely that the effect of CHX was due to a general inhibition of protein synthesis since puromycin, which equally inhibits translation, had an opposite effect (Fig 7B). Furthermore, with the CHX concentrations we used, we did not see a reduction in the ectopic expression of FLAG-TDP-43 A315T or GFP-FUS R495X and CHX was unable to affect miRNA levels when applied to untransfected NSC-34 cells (Appendix Fig S10A–C, related to Fig 7).

miRNAs down-regulation in the SOD1 G93A mouse model of ALS is reversed by enoxacin

We next extended our observations to the SOD1 G93A mouse model of ALS (B6SJL-Tg (SOD1*G93A)1Gur/J mouse strain) (Gurney *et al*, 1994). We detected down-regulation of several miRNAs in SOD1 G93A spinal cords at day 137, relative to the expression of the same miRNAs at day 77. These changes were not observed in age-matched and litter-matched wild-type controls (Appendix Fig S11A related to Fig 8). The mRNA and protein levels of AGO2, DICER, PACT and TRBP remained unchanged (Appendix Fig S11B and C related to Fig 8). The relatively mild reduction may be due to extracting RNA from the whole spinal cord tissue.

Recently, enoxacin was shown to increase the expression of miRNAs in the frontal cortex of rats with beneficial impact on depression (Smalheiser *et al*, 2014). Therefore, we tested whether miRNA levels are changed *in vivo* after oral application of enoxacin ($n = 5$) or carrier (water, $n = 5$) to SOD1 G93A male sibling-matched cohorts. Treatment starting on day 42 of the mouse life did not affect miRNA levels in wild-type motor cortices that were harvested at day 90, relative to controls. However, the levels of several miRNAs were up-regulated by enoxacin in SOD1 G93A motor cortices (Appendix Fig S11D and E related to Fig 8).

Enoxacin therapy is beneficial for neuromuscular function in the SOD1 G93A mouse model of ALS

We next tested whether enoxacin has a beneficial effect on neuromuscular function of SOD1 G93A mice (Gurney *et al*, 1994). We observed a ~7-day delay at the onset of neurological symptoms of the enoxacin-treated group ($n = 40$) relative to sibling-matched male cohort treated with carrier (water, $n = 37$) (Fig 8A). Consistently, weight peak and onset of weight decline, which is defined by the loss of 1 g bodyweight after the weight peak, were delayed in enoxacin-treated mice (Fig 8B and C). Kaplan–Meier survival analysis did not yield significant differences between the two groups (Fig 8D). However, evaluation of neurological status by employing a common neurological scoring system, with numerical values increasing from 0 to 4 as the disease progresses (Gill *et al*, 2009). Neurological scoring revealed that the enoxacin-treated cohort was superior to untreated controls (Fig 8E).

To further evaluate motor function, we performed automated quantitative gait analysis, using the CatWalk system (Neumann *et al*, 2009). Swing speed was significantly higher and stride length was significantly increased in the enoxacin-treated group, relative to untreated controls (ten matched siblings per group, Fig 8F and G). Additionally, the performance of the enoxacin-treated group was superior to untreated siblings in a rotarod test ($n = 25$ control, $n = 29$ enoxacin, Fig 8H). Therefore, enoxacin has a beneficial effect on multiple clinical parameters of the SOD1 G93A mouse model. Furthermore, even a lower enoxacin dose significantly improved gross strength on a hang-wire assay and the clinical neurological score, relative to controls (16 animals treated with enoxacin, 15 untreated controls; Fig 8I and J). Finally, enoxacin-treated animals ($n = 6$) moved significantly more than untreated controls ($n = 5$) in a fully automated infrared-based home cage locomotion assay (Fig 8K). Although enoxacin did not extend the lifespan of the SOD1 G93A model, an array of different assays revealed improved neuromuscular function, suggesting a beneficial profile. Noteworthy, riluzole, the only FDA-approved drug for ALS, lacks survival benefit in SOD1G93A mice (Scott *et al*, 2008; Li *et al*, 2013a). Therefore, as previously suggested (Scott *et al*, 2008), the predictive value of the aggressive SOD1 G93A model may be limited due to its 23 transgene copies in testing novel pharmacological interventions.

We also tested enoxacin in the TDP-43 A315T transgene (Wegorzewska *et al*, 2009). Enoxacin-treated TDP-43 A315T females displayed an improved neurological score, relative to a control cohort (nine treated animals, eight untreated controls; treatment started on day 42; Fig 8L), performed better on the Hang-wire test (Fig 8M) and displayed improved stride length (Fig 8N). Of note, characterization of the TDP-43 A315T mice was performed until the onset of clinical gastro-intestinal pathology, which leads to early death of this TDP-43 A315T mouse line and precludes the full development of ALS (Esmaeili *et al*, 2013).

Discussion

miRNAs function at an intriguing interface of cellular stress and disease (Leung & Sharp, 2007; Mendell & Olson, 2012; Emde & Hornstein, 2014). Accordingly, facets of miRNA malfunction in ALS or frontotemporal dementia were reported in the past: We demonstrated that loss of DICER is sufficient to cause progressive degeneration of spinal motor neurons (Haramati *et al*, 2010). In addition, specific miRNA genes are involved in feedback loops upstream or downstream of FUS (Morlando *et al*, 2012; Dini Modigliani *et al*, 2014) or TDP-43 (Buratti *et al*, 2010; Kawahara & Mieda-Sato, 2012). miRNAs were suggested to regulate neuromuscular junction repair (Williams *et al*, 2009; Valdez *et al*, 2014), to plausibly regulate neuro-inflammation in ALS (Koval *et al*, 2013) and may serve as circulating biomarkers (De Felice *et al*, 2014; reviewed in Droppelmann *et al*, 2014; Gascon & Gao, 2014).

The current work provides novel evidence that global down-regulation of miRNAs is a molecular commonality for genetically unrelated forms of human ALS and suggests that similar previous observations (Campos-Melo *et al*, 2013) are primarily due to changes in miRNA expression in motor neurons.

The observations in human samples led us to investigate the mechanism. We demonstrated that decreased DICER catalytic activity is reducing miRNA levels. Several lines of evidence suggest that DICER complex activity is inhibited by the emergence of SGs: (i) The interaction of several RNA-binding proteins that are normally

 © 2015 The Authors

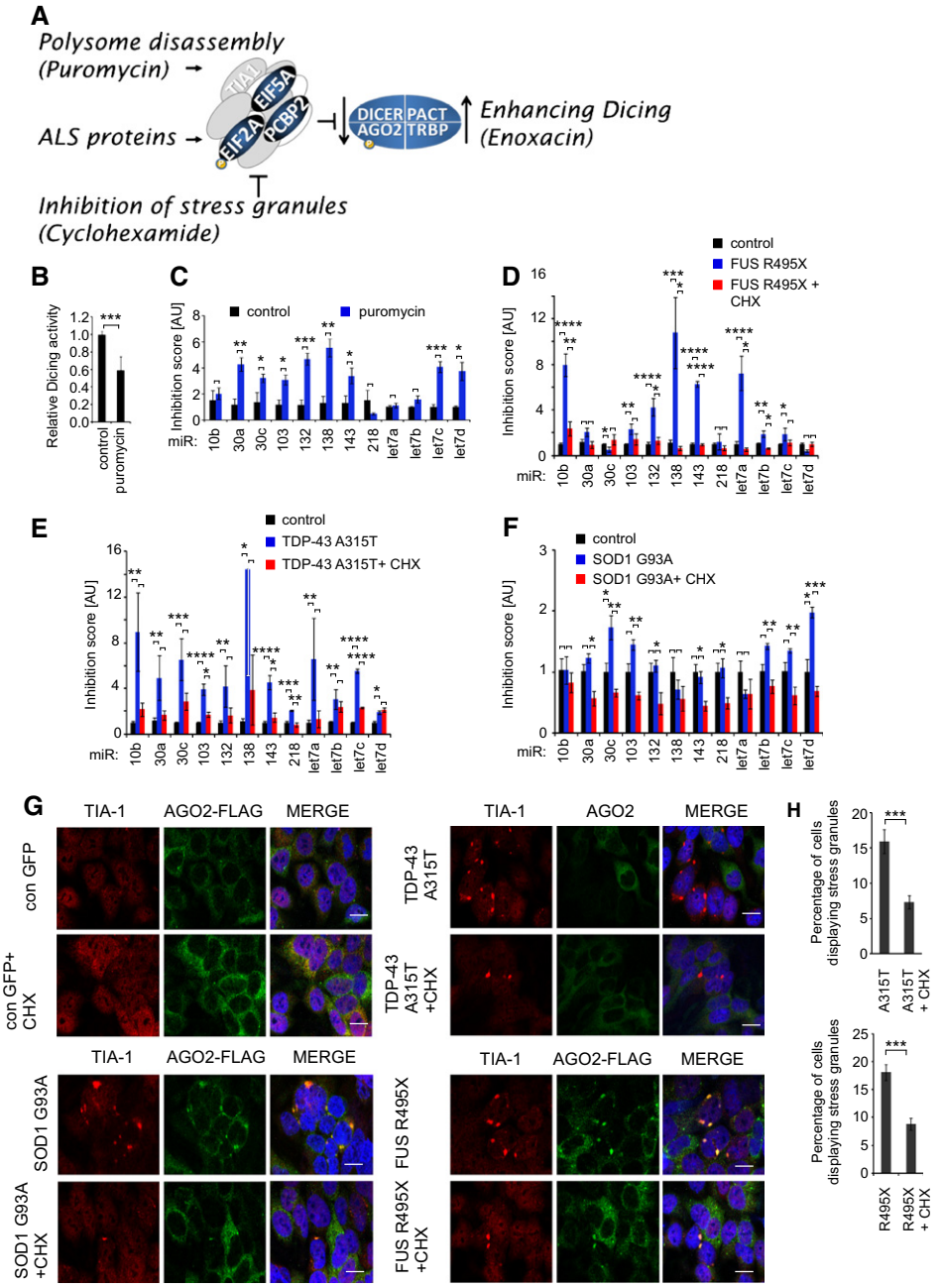

Figure 7. Stress granule formation impacts on Dicing complex efficacy.

A Diagram depicting the working hypothesis that DICER complex activity is attenuated by stress granules that can be initiated by polysome disassembly. Inhibition of DICER activity by overexpression of ALS-causing proteins can be mitigated by inhibiting stress granule formation with cycloheximide or by enhancing DICER activity with enoxacin.

B Dicing *in vitro* assay was performed on lysates of NSC-34 cells, treated with puromycin (1 μg/ml for 24 h) or carrier (water). Average values of > 4 independent biological repeats; error bars represent s.e.m.; ***$P < 0.001$ by two-sided Student's *t*-test.

C–F Inhibition score of individual pre-miRNA:miRNA pairs in NSC-34 cells treated with puromycin (1 μg/ml for 24 h) or carrier (water) (C) or cells transfected with ALS-causing FUS R495X (D), TDP-43 A315T (E) or SOD1 G93A (F) or control vector and treated with low-dose cycloheximide (CHX) (0.02 μg/ml) or carrier (water), starting at 6 h post-transfection. Cells were harvested 72 h post-transfection. Calculated values are based on qPCR analysis of pre-miRNAs and mature miRNAs presented in Appendix Fig S8. Inhibition score was normalized to values in cells transfected with control vector. Averages ± s.e.m.; *$P < 0.05$, **$P < 0.01$, ***$P < 0.001$, ****$P < 0.0001$ by two-sided Student's *t*-test from > 3 independent biological replicates.

G AGO2-FLAG HEK293 cells transfected with FUS R495X or SOD1 G93A and HEK293 transfected with TDP-43 A315T vector versus control plasmid treated with cycloheximide (CHX, 0.02 μg/ml) or carrier and immunostained with antibodies as indicated 72 h post-transfection. Scale bars indicate 10 μm.

H Percentage of HEK293 cells with stress granules overexpressing TDP-43 A315T or FUS R495X in the presence or absence of cycloheximide (0.02 μg/ml for 72 h). Average was calculated from > 100 cells in > 5 pictures per condition; error bars represent s.e.m; ***$P < 0.001$ by two-sided Student's *t*-test.

Source data are available online for this figure.

© 2015 The Authors

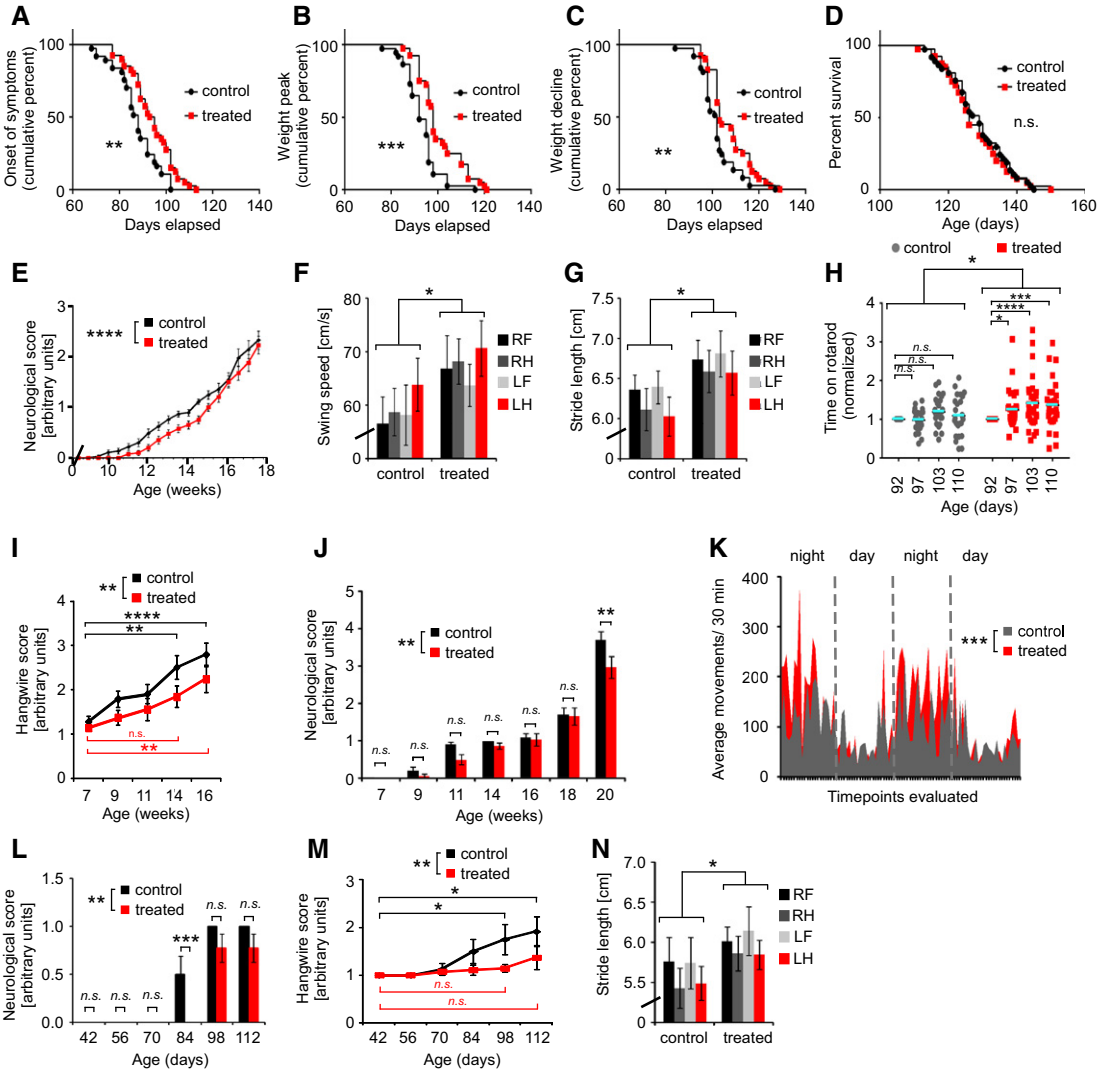

Figure 8. Beneficial impact of enoxacin on neuromuscular function of two different mouse ALS models.

A–H Oral application of enoxacin (800 mg/kg bodyweight/day, $n = 40$) or carrier (water; $n = 37$) to SOD1 G93A male mice started on day 42 of the mouse life. (A) Onset of symptoms (neurological score 1); log-rank Mantel–Cox test, $^{**}P = 0.0025$. (B) Weight peak, log-rank Mantel–Cox test, $^{***}P = 0.0002$. (C) Onset of weight decline, defined as the loss of 1 g bodyweight after the weight peak were measured; log-rank Mantel–Cox test, $^{**}P = 0.0099$. (D) Kaplan–Meier survival plot reveals comparable life span of SOD1 G93A mice, regardless of therapy. Not significant (n.s.), by log-rank Mantel–Cox test. (E) Average neurological score, which increases with disease progression, per cohort ($n = 40$ enoxacin-treated, $n = 37$ controls), two-way ANOVA test, $^{****}P < 0.0001$ (control versus enoxacin). *Post hoc* Holm–Sidak tests did not reveal significant differences comparing control versus enoxacin at single time points. (F, G) Fully automated gait CatWalk analysis with ten matched siblings per group. (F) Four-paw swing speed on day 73, two-way ANOVA $^{*}P = 0.027$ (control versus enoxacin). (G) Four-paw stride length on day 80, two-way ANOVA $^{*}P = 0.012$ (control versus enoxacin). *Post hoc* Holm–Sidak tests did not reveal significant differences when comparing single-paw behavior. (H) Multiple time point rotarod performance, normalized to initial performance at day 92 of each individual ($n = 25$ control, $n = 29$ enoxacin). Two-way ANOVA with repeated measures for each individual, $^{*}P = 0.047$ (control versus enoxacin), followed by *post hoc* Holm–Sidak tests, $^{*}P < 0.05$, $^{***}P < 0.001$, $^{****}P < 0.0001$.

I–K Oral application of enoxacin 200 mg/kg bodyweight/day or carrier (water) to SOD1 G93A male mice started day 42 of the mouse life. (I) Hang-wire assay ($n = 15$ control, $n = 16$ enoxacin), two-way ANOVA (control versus enoxacin) $^{**}P = 0.0027$, followed by *post hoc* Holm–Sidak tests of different time points within groups, $^{**}P < 0.001$, $^{****}P < 0.0001$. Lower hang-wire score indicate greater strength. (J) Neurological score, which increases with disease progression ($n = 15$ control, $n = 16$ enoxacin), two-way ANOVA (control versus enoxacin) $^{**}P = 0.0084$, followed by *post hoc* Holm–Sidak test reveals a significant difference at 20 weeks of age $^{**}P < 0.01$. (K) Fully automated infrared-based home cage locomotion analysis (InfraMot, TSE-Systems) at 30-min intervals over a period of 46 h, days 129–130 ($n = 5$ control, $n = 6$ enoxacin). Two-way ANOVA (control versus enoxacin), $^{***}P = 0.0004$.

L–N Oral application of enoxacin 200 mg/kg bodyweight/day ($n = 9$) or carrier (water; $n = 8$) to TDP-43 A315T females started at day 42 of the mouse life. (L) Onset of symptoms (neurological score 1); two-way ANOVA (control versus enoxacin) $^{**}P = 0.0013$, followed by *post hoc* Holm–Sidak tests reveals $^{***}P < 0.001$ at day 84. (M) Hang-wire assay, two-way ANOVA (control versus enoxacin), $^{**}P = 0.0079$, followed by *post hoc* Holm–Sidak tests of different time points within groups, with $^{*}P < 0.05$. Lower hang-wire scores indicate greater strength. (N) CatWalk analysis revealed better performance, as assessed by four-paw stride length on day 83, two-way ANOVA ($^{*}P = 0.045$). *Post hoc* Holm–Sidak tests did not reveal significances comparing single-paw behavior.

Data information: All error bars, s.e.m. Note that in (A–C, D), *x*-axis starts at days 60 and 100, respectively. Discontinuation of *y*-axis in (F, G, N) is marked by oblique crossing line.
Source data are available online for this figure.

© 2015 The Authors

found in stress granules with DICER or AGO2 increases upon stress. (ii) Initiating SGs by overexpressing EIF5A or TIAR, the phosphomimetic form EIF2A, or by puromycin, was sufficient to reduce DICER activity in cells and in cell lysates. (iii) AGO2, a cofactor of DICER, co-localizes with TIA1 in cytoplasmic SGs after transfection of ALS-causing genes. (iv) Blocking SGs with cycloheximide or with non-phosphorylatable serine-to-alanine 51 mutant of EIF2A reversed the negative effect of ALS-causing mutants on miRNA biogenesis. Puromycin and cycloheximide are two inhibitors of translation, yet they display opposite effects both on pre-miRNA processing and, respectively, on SG formation. Thus, the protective activity of cycloheximide in motor neurons (Yang *et al*, 2013) is consistent with its ability to inhibit SG formation and to improve miRNA biogenesis. (v) These observations are in line with the previous identification of TDP-43 and FUS in SGs and with the fact that TDP-43 binds DICER and AGO2 directly (Kawahara & Mieda-Sato, 2012), providing a conceivable explanation also for the stronger molecular phenotypes observed with TDP-43 and FUS, relative to SOD1.

Therefore, we suggest that stress and SG formation initiate dynamic changes in DICER interactions with its co-factors, in a way that diminishes DICER complex activity. This may be because of acquired or lost interactions under stress and may be related to AGO2 post-translational modifications (Leung *et al*, 2006; Qi *et al*, 2008; Zeng *et al*, 2008; Shen *et al*, 2013) or to increased AGO2 binding to DICER, which counter-intuitively decreases DICER activity (Tahbaz *et al*, 2004).

Enoxacin increases the binding affinity of TRBP to pre-miRNAs, thereby augmenting pre-miRNA processing (Shan *et al*, 2008; Melo *et al*, 2011). We demonstrated that impaired miRNA biogenesis is mitigated by enoxacin with beneficial clinical outcome on the neuromuscular performance of two different ALS mouse models. We did not observe any lifespan extension, but also Riluzole, the only FDA-approved drug for ALS, lacks survival benefit in SOD1 G93A mice (Scott *et al*, 2008; Li *et al*, 2013a). Therefore, as previously suggested (Scott *et al*, 2008), the predictive value of the aggressive SOD1 G93A model may be limited in testing novel pharmacological interventions. Furthermore, SOD1 effect on DICER activity may be more limited than the effects mediated by FUS or TDP-43, which are RNA-binding proteins that are directly engaged in SGs.

Nonetheless, if DICER and miRNAs are indeed instrumental in the pathogenesis of ALS in humans, as we suggest, these observations hold promise for future intervention by validating DICER as a new therapeutic target. Furthermore, enoxacin is a particularly intriguing candidate for clinical assessment, based on its established safety and pharmacokinetic profile and because several forms of ALS converge in the down-regulation of miRNAs. However, more effective DICER agonists might exhibit more dramatic beneficial effects in ALS in the future.

miRNAs impart robustness to cellular programs in development and in the adult life (Hornstein & Shomron, 2006; Pelaez & Carthew, 2012; Cassidy *et al*, 2013; Emde & Hornstein, 2014). Accordingly, even moderate DICER and miRNA insufficiency contributes to failed homeostatic mechanisms, allowing the activation of myriad aberrant pathways that were otherwise repressed under normal miRNA activity. The consequences may contribute particularly to diminished stress resistance, creating a vicious cycle, which further increases neuronal stress up to the threshold of malfunction and death. Accordingly, in one example, even mild but long-term down-regulation of brain-enriched miR-124 affected AMPA expression and frontotemporal dementia phenotype (Gascon *et al*, 2014).

The sensitivity of DICER activity to cellular stress is not limited to motor neurons and may be probably relevant to other tissues under chronic stress, where decrease in miRNA or DICER abundance was reported (Kaneko *et al*, 2011; Mori *et al*, 2012; Inukai & Slack, 2013; Nidadavolu *et al*, 2013). Thus, evaluating whether stress impinges on DICER activity in other disease states will be valuable. The variability in miRNA biogenesis with different stressors or by using different cell types suggests additional factors that are currently unknown.

In summary, we provide evidence for the control of miRNA biogenesis at the level of DICER complex activity, by several stress-related cellular changes. The consecutive reduction in miRNA levels unifies various forms of ALS, suggesting that the development of novel therapies might focus on DICER or miRNAs as common critical effectors of neuronal integrity.

Materials and Methods

Human tissue miRNA analysis

Human nervous tissues were acquired by way of an Investigational Review Board and Health Insurance Portability and Accountability Act compliant process. Sporadic ALS nervous systems were from patients who had met El Escorial criteria for definite ALS. Informed consent was obtained from all subjects. Tissue measurements were carried out post-mortem and conformed to the WMA Declaration of Helsinki and the Department of Health and Human Services Belmont Report. Sporadic ALS nervous systems were from patients who had bulbar or arm-onset disease and caudal progression, and thus, the lumbar regions had relatively abundant residual motor neurons. Tissue collections were as previously described: Completed within 4–6 h of death, the motor system was dissected, embedded in OCT and stored at −80°C. RNA quality was assessed using microelectrophoresis on an Agilent 2100 Bioanalyzer as previously described. Microdissected cell punches were captured on CapSure™ Macro LCM Caps (Arcturus Bioscience). 35 to 50 cryosections were cut at a thickness of 9 μm in a −18°C cryotome and placed onto uncharged glass slides. The sections were returned to −80°C for a minimum of 3 h. They were stained with cresyl violet acetate in a 10-step, timed, nuclease-free immersion process. Motor neurons were microdissected using a Pixcell IIe Laser Capture Microdissection (LCM) System (Arcturus Bioscience) and CapSureTM Macro LCM Caps (Applied Biosystems). Each LCM session collected 500–1,000 motor neuron punches and lasted < 2.5 h. Total RNA was isolated using the RNAqueous Micro kit (Life Technologies) as per the manufacturer's procedure. RNA quality was assessed by spectrophotometric analysis using a Nanodrop ND-1000 spectrophotometer and an Agilent 2100 Bioanalyzer. Expression of 667 microRNAs was assessed using the microRNA TaqMan® qPCR Megaplex pools array on an ABI 7900HT Fast Real-Time PCR System (Life Technologies). Technical replicates were run after pre-amplification using the manufacturer's protocol. Relative quantification was calculated by comparing arithmetic mean of three small RNA control genes nucleolar RNU48/SNORD48,

© 2015 The Authors

RNU44/SNORD44 and splicosome-related U6. Two-way ANOVA test was performed with DataAssist Software (Life technologies Inc.). *In situ* hybridization was performed on 7-μm sections of frozen spinal tissue from lumbar regions, briefly fixed in 4% paraformaldehyde and incubated in 2 μg/ml proteinase K. Slides were then incubated for 10 min in 0.13 M 1-methylimidazole (Sigma), 300 mM NaCl, pH 8.0 and further fixed in EDC (Sigma) following Pena *et al* (2009), acetylated for 30 min in a solution of freshly prepared 0.1 M triethanolamine and 0.5% (v/v) acetic anhydride. Hybridization of sections with 4 pmol of 5′ and 3′ DIG-labeled miR-9 and miR-124 LNA probes followed manufacturer's instructions (Exiqon).

Tissue culture vectors and small molecules

HEK293 cells (American Type Culture Collection) and NSC-34 cells (Cellutions Biosystems Inc.) were cultured in high-glucose DMEM (Gibco), 1% L-glutamine, 10% fetal calf serum and 1% penicillin/streptavidin. Mouse embryonic fibroblasts (MEFs) were cultured in DMEM (Gibco), 15% fetal calf serum, L-glutamine, 1% penicillin/streptavidin and sodium pyruvate. AGO2-FLAG-expressing HEK293 cells were a gift of Markus Landthaler. EIF2A S51A mouse embryonic fibroblasts were provided by Prof. Chaim Kahana, Weizmann Institute of Science, Israel. Mouse embryonic motor neurons were harvested as described in Milligan and Gifondorwa (2011). Expression vectors are as follows: EIF2A 3 (S51D) from David Ron (Addgene plasmid # 21809); pBabe_puro_DEST_Flag_EIF5A2 from William Hahn (Addgene plasmid # 45266); and pLJM60-Tiar from David Sabatini (Addgene plasmid # 38244). Wild-type and R495X FUS vector were provided by Daryl Bosco (University of Massachusetts, Boston), wild-type and A315T TDP-43 vectors by Markus Landthaler (MDC Berlin, Germany), and wild-type and G93A SOD1 vectors by Yoram Groner (WIS, Israel). DICER-FLAG and AGO2-FLAG plasmids were kindly provided by Narry Kim (Seoul National University, South Korea). Enoxacin was supplied by Sigma-Aldrich (E3764-5G) or Buckton-Scott (Germany). Thapsigargin, paraquat, cycloheximide and puromycin are purchased from Sigma-Aldrich, Israel.

RNA analysis

RNA was extracted using Tri reagent (Molecular Research Center Inc.) or Qiazol with consecutive use of the miRNeasy Mini Kit (Qiagen). Pre-miRNA and miRNA reverse transcription was performed using miScript Kits No. I & II (Qiagen). Quantitative analysis of miRNA and pre-miRNA expression was performed in > 3 independent biological repeats and additionally in technical duplicates with StepOnePlus quantitative Real-Time PCR System, and two-way ANOVA test was performed with DataAssist Software (Life technologies Inc.). Primers are described in Table EV1 and additional pre-miRNA sequences are from Jiang *et al* (2005).

Cell-free dicing assay

Dicing assay is described in Melo and Melo (2014) with the following modifications: dsRNA substrate for measuring DICER activity was annealed from 5′Phos/mCmU rCmArU mUrUrC rCrUrG mGrUmA rUmGrA mCrArA rCrGrA mAmU/3′IABkFQ and 5′Cy3/mAmU mUrCrG rUrUrG mUrCmA rUmArC rCrArG rGrArA rArUmG rAmGmC rU (Integrated DNA Technologies). Cells were lysed via sonication in hypotonic solution, with consecutive DICER assay reaction assembly by mixing 3 μl of 10× Buffer K (200 mM Hepes–KOH, pH 7.0, 20 mM dithiothreitol (DTT), 20 mM $MgCl_2$); 3 μl of 10 mM ATP; 1.5 μl of 0.5 M, freshly dissolved, creatine phosphate; 0.9 μl of 1 mg/ml creatine phosphate kinase; 0.6 μl of ribonuclease inhibitor (40 units/μl); 3 μl of labeled dsRNA (50 nM); and 18 μl of cell extract. DICER assay mix was incubated at 30°C for 2 h and diluted with 100 μl of ultra-pure water, and then, 10 μl was transferred to 384-multiwell plate (10 technical repeats for each reaction) and measured on PHERAstar FS microplate reader (BMG Labtech). Pre-annealed ssRNA Cy3 fluorescent oligo served as positive control for calibration curve. Annealed and quenched dsRNA without cell extract served as negative control for quantification of background fluorescence.

Western blot analysis

Cell extracts or immune-purified proteins were eluted by boiling in X5 sample buffer (60 mM Tris–HCl pH 6.8, 25% glycerol, 2% SDS, 14.4 mM β-mercaptoethanol, 0.1% bromophenol blue) for 5 min. The samples were separated via 8% SDS–polyacrylamide gel electrophoresis at 120 V for 70 min, electro-transferred onto nitrocellulose membrane (Whatmann, 10401383) at 100 V for 1 h, stained with Ponceau (Sigma, P7170) to asses transfer quality and then blocked for 1 h at room temperature with 5% milk protein in PBS + 0.05% Tween-20 (0.05% PBST). Blocked membranes were then incubated with shaking at 4°C overnight with primary antibodies in 5% bovine serum albumin, 0.02% sodium azide and five drops of phenol red in 0.05% PBST. Membranes were next washed 3 times for 5 min at room temperature with 0.05% PBST and then incubated with horseradish peroxidase-conjugated species-specific secondary antibodies in 5% milk for 1 h at room temperature. Membranes were washed three times for 5 min in 0.05% PBST and visualized by ImageQuant™ LAS 4000 (GE Healthcare Life Sciences) using EZ-ECL Chemiluminescence detection kit (Biological Industries, 20-500-120). Primary antibodies used are as follows: anti-DICER (ab13502) 1:500; anti-AGO2 (ab32381) 1:500; anti-PACT (ab75749) 1:1,000; anti-TRBP (ab42018) 1:1,000; anti-PCBP1 (ab74793) 1:1,000 from Abcam; anti-GAPDH (Ambion, AM4300) 1:4,000; anti-phospho-eIF2α (Ser51) (Cat# 04-342EMD, Millipore) 1:500; anti-eIF2α (sc-11386, Santa Cruz Biotechnology) 1:200; anti-TLS/FUS (cat. 611385, BD Transduction Laboratories) 1:500; and anti-TDP-43 (10782-2-AP, Proteintech) 1:1,000.

Mass spectrometry

For mass spectrometry, HEK293 cells that stably express AGO2-FLAG ($n = 3$ for each group) or DICER-FLAG-transfected cells (48 h post-transfection, $n = 4$ for each group) were untreated or stressed with 0.5 mM sodium arsenite for 60 min before harvest. IP was performed with the FLAG-IPT1 Kit (Sigma-Aldrich). Negative controls were HEK293 cells not containing a FLAG construct. Eluted proteins and the FLAG peptide were filtered using 3-kDa molecular weight cutoff spin columns (Amicon, Millipore). Buffer was exchanged to 50 mM ammonium bicarbonate (Sigma-Aldrich) in the same step. Proteins were reduced by addition of dithiothreitol (Sigma-Aldrich) to a final concentration of 5 mM and incubation for 30 min at 60°C and

 © 2015 The Authors

alkylated with 10 mM iodoacetamide (Sigma-Aldrich) in the dark for 30 min at 21°C. The proteins were then digested using trypsin (Promega; Madison, WI, USA) at a ratio of 1:50 (w/w trypsin/protein) for 16 h at 37°C. Digestion was stopped by addition of 1% trifluoroacetic acid (TFA). Samples were stored in −80°C until analysis. Each sample was spiked with the mixture of 51 heavy isotopically labeled peptides (JPT Technologies). Heavy labels included U-$^{13}C_6$; U-$^{15}N_4$ for peptides terminating with Arg and U-$^{13}C_6$; U-$^{15}N_2$ for Lys. ULC/MS grade solvents were used for all chromatographic steps. Each sample was loaded using split-less nano-ultra-performance liquid chromatography (10k psi nanoAcquity; Waters, Milford, MA, USA). Mobile phase was as follows: A) H_2O + 0.1% formic acid and B) acetonitrile + 0.1% formic acid. Desalting of samples was performed online using a reverse-phase C18 trapping column (180 μm i.d., 20 mm length, 5 μm particle size; Waters). The peptides in samples were separated using a C18 T3 HSS nano-column (75 μm i.d., 250 mm length, 1.8 μm particle size; Waters) at 0.3 μl/min. Peptides were eluted from the column and into the mass spectrometer using the following gradient: 3–30% B in 90 min, 30–35% in 10 min, 35–90% B in 5 min, maintained at 90% for 5 min and then back to initial conditions. The analytical column was coupled with a quadruple orbitrap mass spectrometer (Q Exactive, Thermo Scientific), via a nano-ESI interface. Parallel reaction monitoring of mass spectrometry (MS) was according to Peterson *et al* (2012) at maximum injection time of 300 ms, resolution of 35,000 and target automatic gain control (AGC) of 2e5. Samples were analyzed in a random order, measuring the light and heavy forms of each target peptide. Data were processed with Skyline software (MacLean *et al*, 2010). Extracted ion chromatograms were integrated, and the ratio of the light to heavy forms was calculated. Student's *t*-test was used, after logarithmic transformation, for statistical calculations of the differential peptide expression. Peptide sequences for mass spectrometry are described in Table EV1.

Immunocytofluorescence microscopy

Wild-type or stably transfected AGO2-FLAG HEK293 cells were cultured on poly-A-lysin-coated coverslips and further subjected to transfection or treated with stress-inducing chemicals. For microscopy, cells on coverslips were rinsed with PBS, fixed with 4% formaldehyde, permeabilized with 0.1% Triton X-100 (Sigma-Aldrich, St. Louis, MO), blocked with PBS, 2% BSA and incubated with anti-TIA1 antibody (sc-1757, Santa Cruz Biotechnology), anti-Flag antibody (F1804, Sigma-Aldrich) and anti-AGO2 (ab32381, Abcam) overnight. Coverslips were washed three times with PBS and incubated with secondary antibodies (Cy2 donkey anti-goat 705-495-147 and Cy5 donkey anti-mouse 715-175-150, Jackson Immunoresearch) for 1 h. Coverslips were washed 3 times with PBS, mounted with Fluoroshield™ with DAPI (F6057, Sigma) and captured with a LSM 710 confocal microscope (Carl Zeiss AG).

In vivo enoxacin study

All experiments were performed according to Weizmann Institute of Science guidelines and IACUC approval (protocol No. 03040512-1). Mice, B6SJL-Tg(SOD1*G93A)1Gur/J, which were first reported in Gurney *et al* (1994), carry a hemizygous high transgene copy number of the SOD1 G93A mutant on a B6SJL hybrid background (Jackson Laboratories, 002726). The TDP-43 A315T mouse line (Wegorzewska *et al*, 2009) was on a C57BL/6J background (Jackson Laboratories, 010700). All experiments were performed sibling-matched, except the mice in the 200 mg/kg bodyweight SOD1 G93A enoxacin group, in which mice were randomly assigned to treatment groups. Animals were group-housed on a 12-h light–dark cycle. Food and water were provided *ad libitum*. Food pellets at cage floor, long sipper tubes on bottles and nutrient gel were used to ease accessibility to nutrition when mice deteriorated according to Gill *et al* (2009). RotaRod™ performance (San Diego Instruments) was evaluated at ramp speed 4, 40 rpm. Data are presented as the average latency to fall off the rotarod of three independent rounds per time point and are normalized to average initial performance at pre-symptomatic stage for each individual for each time point. A fully automated gait analysis with the CatWalk XT™ (Noldus) system was performed. Data were obtained of > 4 independent rounds on the apparatus. For hang-wire muscle strength assessment, mice were allowed forelimb grip onto a 2-mm-thick horizontal metal wire, suspended 80 cm above surface. Ability to successfully raise hindlimbs to grip the wire and crawling to the end of the wire was scored: 1 = successful four-paw grip and crawling to the end of the wire within < 60 s; 2 = four-paw grip for > 15 s without crawling; 3 = failure to successfully establish hindlimb grip in 60 s; and 4 = inability to sustain forelimb grip for 60 s. Each mouse was evaluated in two sessions on two consecutive days, consisting of three trials each, with a 15-min inter-trial interval. The second day was used to obtain the data as displayed. Neurological score was assessed according to Gill *et al* (2009): 0 = > 2 s extension of hindlimbs away from lateral midline when mouse is suspended by its tail 2–3 times; 1 = collapse or partial leg collapse toward midline or hind leg trembling during tail suspension; 2 = toes curl under at least twice during a 12-inch walk, or any part of foot is dragging along cage/table bottom; 3 = rigid paralysis or minimal joint movement, foot not being used for forward motion; and 4 = humane endpoint, mouse cannot right itself within 30 s on either side. The locomotion of animals was quantified over a period of 46 h in the home cage, by automated sensing of body-heat image using an InfraMot (TSE-Systems). Individual animal movements were summed up every 30 min. Animal statistics: rotarod performance was evaluated using the two-way ANOVA with repeated measures for each individual and *post hoc* Sidak–Holm tests. Weight peak, weight decline, onset of symptoms and survival were calculated with log-rank (Mantel–Cox) test. All other tests employed two-way ANOVA with *post hoc* Sidak–Holm tests. All animal statistics were calculated with GraphPad Prism 6 statistics program.

Expanded View for this article is available online:
http://emboj.embopress.org

Acknowledgements

We thank Ranjan Batra (University of California, SD) for sharing bioinformatics analysis from ongoing studies; Markus Landthaler (Max Delbrück Center for Molecular Medicine), Daryl Bosco (University of Massachusetts, Boston), Zissimos Mourelatos (University of Pennsylvania), Yoram Groner, Menachem Rubinstein, Ari Elson (Weizmann Institute of Science), David Ron (CIMR, University of Cambridge), William Hahn (Dana Farber Cancer Institute, HMS) and David Sabatini (Whitehead Institute, MIT) for vectors and reagents; Pat

© 2015 The Authors

Janssen and Fred Farin (UW Functional Genomics and Bioinformatics Core Laboratory) for technical assistance and troubleshooting; and Tal Yardeni (Weizmann Institute of Science) for whole spinal cord RNA. We further thank Daniel Dar (Weizmann Institute of Science) for RNA analysis, Chaim Kahana (Weizmann Institute of Science), Orna Elroy-Stein (Tel Aviv University), Markus Weber (Kantonsspital St. Gallen), Witold Filipowicz (FMI, Basel), Bernard Schneider (EPFL, Lausanne), Mark A. Behlke (Integrated DNA Technologies, Inc.) and Peter Andersen (Umea University) for discussions and advice and Danielle Aronowitz for English editing. This work was supported by grants to E.H. from the Israel Science Foundation, the ISF Legacy-heritage Program, The Bruno and Ilse Frick Foundation for Research on ALS, Yeda-Sela, Yeda-CEO fund, Minna-James-Heineman Stiftung through Minerva, ERC Consolidator Program, Israel Ministry of Industry, Trade and Labor "Kamin Program", Nella and Leon Benoziyo Center for Neurological Diseases, Y. Leon Benoziyo Institute for Molecular Medicine and the ALS-Therapy Alliance. Additional funding was from Kekst Family Institute for Medical Genetics, David and Fela Shapell Family Center for Genetic Disorders Research, Crown Human Genome Center, Nathan, Shirley, Philip and Charlene Vener New Scientist Fund, Julius and Ray Charlestein Foundation, Fraida Foundation, Wolfson Family Charitable Trust, Adelis Foundation, MERCK UK, Maria Halphen, Estates of Fannie Sherr, Lola Asseof, Lilly Fulop, The "National Network of Excellence in Neuroscience" (NNE), initiated by Teva and miCure Therapeutics. Grants to T.M. from the ALS Association (grant 1765); to L-L.L. from NIH T32 fellowship NS051171; and to J.R. by Microsoft Research, the family of T. Evans Wyckoff, the friends of Greg Brooks, and Lois Caprile. A.E. was supported by Deutsche Forschungsgemeinschaft. E.H. was the incumbent of the Milton A. Kimmelman Career Development Chair, and the Hornstein Laboratory is further supported by Dr. Sidney Brenner and friends.

Author contributions

AE conceived and led the research, performed all non-human experimental activities and data analysis, including molecular biology and animal studies. RTL and JMR provided human autopsy material. L-LL, ASi and BA performed laser capture microdissection and human tissue RNA analysis. CE performed protein quantification studies. NR performed microscopic studies, developed and performed *in vitro* DICER assays. HO and RE performed miRNA *in situ* hybridization study. ASa and YL performed mass spectrometry. IR, JA, IM, RS, IZB-D and SMH helped conducting research or provided critical input for scientific interpretations. JMR, TM and EH conceived research and supervised the study. AE and EH developed the interpretations presented and wrote the manuscript with comments from JMR and TM. JMR is the corresponding author for the human analysis, and EH is the corresponding author for all other facets of the study. TM and EH share senior authorship.

Conflict of interest

The authors declare that they have no conflict of interest.

References

Anderson P, Kedersha N (2008) Stress granules: the Tao of RNA triage. *Trends Biochem Sci* 33: 141 – 150

Anderson P, Kedersha N (2009) RNA granules: post-transcriptional and epigenetic modulators of gene expression. *Nat Rev Mol Cell Biol* 10: 430 – 436

Aulas A, Stabile S, Vande Velde C (2012) Endogenous TDP-43, but not FUS, contributes to stress granule assembly via G3BP. *Mol Neurodegener* 7: 54

Baron DM, Kaushansky LJ, Ward CL, Sama RR, Chian RJ, Boggio KJ, Quaresma AJ, Nickerson JA, Bosco DA (2013) Amyotrophic lateral sclerosis-linked FUS/TLS alters stress granule assembly and dynamics. *Mol Neurodegener* 8: 30

Blobel G, Sabatini D (1971) Dissociation of mammalian polyribosomes into subunits by puromycin. *Proc Natl Acad Sci USA* 68: 390 – 394

Bosco DA, Lemay N, Ko HK, Zhou H, Burke C, Kwiatkowski TJ Jr, Sapp P, McKenna-Yasek D, Brown RH Jr, Hayward LJ (2010) Mutant FUS proteins that cause amyotrophic lateral sclerosis incorporate into stress granules. *Hum Mol Genet* 19: 4160 – 4175

Buchan JR, Parker R (2009) Eukaryotic stress granules: the ins and outs of translation. *Mol Cell* 36: 932 – 941

Buratti E, De Conti L, Stuani C, Romano M, Baralle M, Baralle F (2010) Nuclear factor TDP-43 can affect selected microRNA levels. *FEBS J* 277: 2268 – 2281

Campos-Melo D, Droppelmann CA, He Z, Volkening K, Strong MJ (2013) Altered microRNA expression profile in Amyotrophic Lateral Sclerosis: a role in the regulation of NFL mRNA levels. *Mol Brain* 6: 26

Cassidy JJ, Jha AR, Posadas DM, Giri R, Venken KJ, Ji J, Jiang H, Bellen HJ, White KP, Carthew RW (2013) miR-9a minimizes the phenotypic impact of genomic diversity by buffering a transcription factor. *Cell* 155: 1556 – 1567

Chendrimada TP, Gregory RI, Kumaraswamy E, Norman J, Cooch N, Nishikura K, Shiekhattar R (2005) TRBP recruits the Dicer complex to Ago2 for microRNA processing and gene silencing. *Nature* 436: 740 – 744

Costa-Mattioli M, Gobert D, Stern E, Gamache K, Colina R, Cuello C, Sossin W, Kaufman R, Pelletier J, Rosenblum K, Krnjevic K, Lacaille JC, Nader K, Sonenberg N (2007) eIF2alpha phosphorylation bidirectionally regulates the switch from short- to long-term synaptic plasticity and memory. *Cell* 129: 195 – 206

Daigle JG, Lanson NA Jr, Smith RB, Casci I, Maltare A, Monaghan J, Nichols CD, Kryndushkin D, Shewmaker F, Pandey UB (2013) RNA-binding ability of FUS regulates neurodegeneration, cytoplasmic mislocalization and incorporation into stress granules associated with FUS carrying ALS-linked mutations. *Hum Mol Genet* 22: 1193 – 1205

De Felice B, Annunziata A, Fiorentino G, Borra M, Biffali E, Coppola C, Cotrufo R, Brettschneider J, Giordana ML, Dalmay T, Wheeler G, D'Alessandro R (2014) miR-338-3p is over-expressed in blood, CFS, serum and spinal cord from sporadic amyotrophic lateral sclerosis patients. *Neurogenetics* 15: 243 – 253

Dewey CM, Cenik B, Sephton CF, Dries DR, Mayer P III, Good SK, Johnson BA, Herz J, Yu G (2011) TDP-43 is directed to stress granules by sorbitol, a novel physiological osmotic and oxidative stressor. *Mol Cell Biol* 31: 1098 – 1108

Dewey CM, Cenik B, Sephton CF, Johnson BA, Herz J, Yu G (2012) TDP-43 aggregation in neurodegeneration: are stress granules the key? *Brain Res* 1462: 16 – 25

Dini Modigliani S, Morlando M, Errichelli L, Sabatelli M, Bozzoni I (2014) An ALS-associated mutation in the FUS 3′-UTR disrupts a microRNA-FUS regulatory circuitry. *Nat Commun* 5: 4335

Dormann D, Rodde R, Edbauer D, Bentmann E, Fischer I, Hruscha A, Than ME, Mackenzie IR, Capell A, Schmid B, Neumann M, Haass C (2010) ALS-associated fused in sarcoma (FUS) mutations disrupt Transportin-mediated nuclear import. *EMBO J* 29: 2841 – 2857

Droppelmann CA, Wang J, Campos-Melo D, Keller B, Volkening K, Hegele RA, Strong MJ (2013) Detection of a novel frameshift mutation and regions with homozygosis within ARHGEF28 gene in familial amyotrophic lateral sclerosis. *Amyotroph Lateral Scler Frontotemporal Degener* 14: 444 – 451

 © 2015 The Authors

Droppelmann CA, Campos-Melo D, Ishtiaq M, Volkening K, Strong MJ (2014) RNA metabolism in ALS: when normal processes become pathological. *Amyotroph Lateral Scler Frontotemporal Degener* 15: 321 – 336

Emde A, Hornstein E (2014) miRNAs at the interface of cellular stress and disease. *EMBO J* 33: 1428 – 1437

Esmaeili MA, Panahi M, Yadav S, Hennings L, Kiaei M (2013) Premature death of TDP-43 (A315T) transgenic mice due to gastrointestinal complications prior to development of full neurological symptoms of amyotrophic lateral sclerosis. *Int J Exp Pathol* 94: 56 – 64

Freischmidt A, Muller K, Ludolph AC, Weishaupt JH (2013) Systemic dysregulation of TDP-43 binding microRNAs in amyotrophic lateral sclerosis. *Acta Neuropathol Commun* 1: 42

Fujimura K, Kano F, Murata M (2008) Identification of PCBP2, a facilitator of IRES-mediated translation, as a novel constituent of stress granules and processing bodies. *RNA* 14: 425 – 431

Fujimura K, Katahira J, Kano F, Yoneda Y, Murata M (2009) Selective localization of PCBP2 to cytoplasmic processing bodies. *Biochim Biophys Acta* 1793: 878 – 887

Gal J, Zhang J, Kwinter DM, Zhai J, Jia H, Jia J, Zhu H (2010) Nuclear localization sequence of FUS and induction of stress granules by ALS mutants. *Neurobiol Aging* 32: 2323. e27-40

Gascon E, Gao FB (2014) The emerging roles of microRNAs in the pathogenesis of frontotemporal dementia-amyotrophic lateral sclerosis (FTD-ALS) spectrum disorders. *J Neurogenet* 28: 30 – 40

Gascon E, Lynch K, Ruan H, Almeida S, Verheyden JM, Seeley WW, Dickson DW, Petrucelli L, Sun D, Jiao J, Zhou H, Jakovcevski M, Akbarian S, Yao WD, Gao FB (2014) Alterations in microRNA-124 and AMPA receptors contribute to social behavioral deficits in frontotemporal dementia. *Nat Med* 20: 1444 – 1451

Gill A, Kidd J, Vieira F, Thompson K, Perrin S (2009) No benefit from chronic lithium dosing in a sibling-matched, gender balanced, investigator-blinded trial using a standard mouse model of familial ALS. *PLoS ONE* 4: e6489

Gitcho MA, Baloh RH, Chakraverty S, Mayo K, Norton JB, Levitch D, Hatanpaa KJ, White CL III, Bigio EH, Caselli R, Baker M, Al-Lozi MT, Morris JC, Pestronk A, Rademakers R, Goate AM, Cairns NJ (2008) TDP-43 A315T mutation in familial motor neuron disease. *Ann Neurol* 63: 535 – 538

Gregory RI, Yan KP, Amuthan G, Chendrimada T, Doratotaj B, Cooch N, Shiekhattar R (2004) The microprocessor complex mediates the genesis of microRNAs. *Nature* 432: 235 – 240

Gurney ME, Pu H, Chiu AY, Dal Canto MC, Polchow CY, Alexander DD, Caliendo J, Hentati A, Kwon YW, Deng HX, Chen W, Zhai P, Sufit RL, Siddique T (1994) Motor neuron degeneration in mice that express a human Cu,Zn superoxide dismutase mutation. *Science* 264: 1772 – 1775

Haase AD, Jaskiewicz L, Zhang H, Laine S, Sack R, Gatignol A, Filipowicz W (2005) TRBP, a regulator of cellular PKR and HIV-1 virus expression, interacts with Dicer and functions in RNA silencing. *EMBO Rep* 6: 961 – 967

Haramati S, Chapnik E, Sztainberg Y, Eilam R, Zwang R, Gershoni N, McGlinn E, Heiser PW, Wills AM, Wirguin I, Rubin LL, Misawa H, Tabin CJ, Brown R Jr, Chen A, Hornstein E (2010) miRNA malfunction causes spinal motor neuron disease. *Proc Natl Acad Sci USA* 107: 13111 – 13116

Hinnebusch AG (2005) eIF2alpha kinases provide a new solution to the puzzle of substrate specificity. *Nat Struct Mol Biol* 12: 835 – 838

Hornstein E, Shomron N (2006) Canalization of development by microRNAs. *Nat Genet* 38(Suppl): S20 – S24

Igaz LM, Kwong LK, Lee EB, Chen-Plotkin A, Swanson E, Unger T, Malunda J, Xu Y, Winton MJ, Trojanowski JQ, Lee VM (2011) Dysregulation of the ALS-associated gene TDP-43 leads to neuronal death and degeneration in mice. *J Clin Investig* 121: 726 – 738

Inukai S, Slack F (2013) MicroRNAs and the genetic network in aging. *J Mol Biol* 425: 3601 – 3608

Jaarsma D, Haasdijk ED, Grashorn JA, Hawkins R, van Duijn W, Verspaget HW, London J, Holstege JC (2000) Human Cu/Zn superoxide dismutase (SOD1) overexpression in mice causes mitochondrial vacuolization, axonal degeneration, and premature motoneuron death and accelerates motoneuron disease in mice expressing a familial amyotrophic lateral sclerosis mutant SOD1. *Neurobiol Dis* 7: 623 – 643

Jiang J, Lee EJ, Gusev Y, Schmittgen TD (2005) Real-time expression profiling of microRNA precursors in human cancer cell lines. *Nucleic Acids Res* 33: 5394 – 5403

Kabashi E, Valdmanis PN, Dion P, Spiegelman D, McConkey BJ, Vande Velde C, Bouchard JP, Lacomblez L, Pochigaeva K, Salachas F, Pradat PF, Camu W, Meininger V, Dupre N, Rouleau GA (2008) TARDBP mutations in individuals with sporadic and familial amyotrophic lateral sclerosis. *Nat Genet* 40: 572 – 574

Kaneko H, Dridi S, Tarallo V, Gelfand BD, Fowler BJ, Cho WG, Kleinman ME, Ponicsan SL, Hauswirth WW, Chiodo VA, Kariko K, Yoo JW, Lee DK, Hadziahmetovic M, Song Y, Misra S, Chaudhuri G, Buaas FW, Braun RE, Hinton DR *et al* (2011) DICER1 deficit induces Alu RNA toxicity in age-related macular degeneration. *Nature* 471: 325 – 330

Kawahara Y, Mieda-Sato A (2012) TDP-43 promotes microRNA biogenesis as a component of the Drosha and Dicer complexes. *Proc Natl Acad Sci USA* 109: 3347 – 3352

Kedersha NL, Gupta M, Li W, Miller I, Anderson P (1999) RNA-binding proteins TIA-1 and TIAR link the phosphorylation of eIF-2 alpha to the assembly of mammalian stress granules. *J Cell Biol* 147: 1431 – 1442

Kedersha N, Cho MR, Li W, Yacono PW, Chen S, Gilks N, Golan DE, Anderson P (2000) Dynamic shuttling of TIA-1 accompanies the recruitment of mRNA to mammalian stress granules. *J Cell Biol* 151: 1257 – 1268

Kedersha N, Stoecklin G, Ayodele M, Yacono P, Lykke-Andersen J, Fritzler MJ, Scheuner D, Kaufman RJ, Golan DE, Anderson P (2005) Stress granules and processing bodies are dynamically linked sites of mRNP remodeling. *J Cell Biol* 169: 871 – 884

Kim HJ, Kim NC, Wang YD, Scarborough EA, Moore J, Diaz Z, MacLea KS, Freibaum B, Li S, Molliex A, Kanagaraj AP, Carter R, Boylan KB, Wojtas AM, Rademakers R, Pinkus JL, Greenberg SA, Trojanowski JQ, Traynor BJ, Smith BN *et al* (2013) Mutations in prion-like domains in hnRNPA2B1 and hnRNPA1 cause multisystem proteinopathy and ALS. *Nature* 495: 467 – 473

Kim HJ, Raphael AR, LaDow ES, McGurk L, Weber RA, Trojanowski JQ, Lee VM, Finkbeiner S, Gitler AD, Bonini NM (2014) Therapeutic modulation of eIF2alpha phosphorylation rescues TDP-43 toxicity in amyotrophic lateral sclerosis disease models. *Nat Genet* 46: 152 – 160

Koval ED, Shaner C, Zhang P, du Maine X, Fischer K, Tay J, Chau BN, Wu GF, Miller TM (2013) Method for widespread microRNA-155 inhibition prolongs survival in ALS-model mice. *Hum Mol Genet* 22: 4127 – 4135

Kwiatkowski TJ Jr, Bosco DA, Leclerc AL, Tamrazian E, Vanderburg CR, Russ C, Davis A, Gilchrist J, Kasarskis EJ, Munsat T, Valdmanis P, Rouleau GA, Hosler BA, Cortelli P, de Jong PJ, Yoshinaga Y, Haines JL, Pericak-Vance MA, Yan J, Ticozzi N *et al* (2009) Mutations in the FUS/TLS gene on chromosome 16 cause familial amyotrophic lateral sclerosis. *Science* 323: 1205 – 1208

Lee Y, Hur I, Park SY, Kim YK, Suh MR, Kim VN (2006) The role of PACT in the RNA silencing pathway. *EMBO J* 25: 522 – 532

© 2015 The Authors

Lee HY, Doudna JA (2012) TRBP alters human precursor microRNA processing *in vitro*. *RNA* 18: 2012 – 2019

Lee HY, Zhou K, Smith AM, Noland CL, Doudna JA (2013) Differential roles of human Dicer-binding proteins TRBP and PACT in small RNA processing. *Nucleic Acids Res* 41: 6568 – 6576

Leung AK, Calabrese JM, Sharp PA (2006) Quantitative analysis of Argonaute protein reveals microRNA-dependent localization to stress granules. *Proc Natl Acad Sci USA* 103: 18125 – 18130

Leung AK, Sharp PA (2007) microRNAs: a safeguard against turmoil? *Cell* 130: 581 – 585

Leung AK, Sharp PA (2010) MicroRNA functions in stress responses. *Mol Cell* 40: 205 – 215

Li CH, Ohn T, Ivanov P, Tisdale S, Anderson P (2010) eIF5A promotes translation elongation, polysome disassembly and stress granule assembly. *PLoS ONE* 5: e9942

Li Y, Lin L, Li Z, Ye X, Xiong K, Aryal B, Xu Z, Paroo Z, Liu Q, He C, Jin P (2012) Iron homeostasis regulates the activity of the microRNA pathway through poly(C)-binding protein 2. *Cell Metab* 15: 895 – 904

Li J, Sung M, Rutkove SB (2013a) Electrophysiologic biomarkers for assessing disease progression and the effect of riluzole in SOD1 G93A ALS mice. *PLoS ONE* 8: e65976

Li YR, King OD, Shorter J, Gitler AD (2013b) Stress granules as crucibles of ALS pathogenesis. *J Cell Biol* 201: 361 – 372

Ling SC, Polymenidou M, Cleveland DW (2013) Converging mechanisms in ALS and FTD: disrupted RNA and protein homeostasis. *Neuron* 79: 416 – 438

Liu-Yesucevitz L, Bilgutay A, Zhang YJ, Vanderweyde T, Citro A, Mehta T, Zaarur N, McKee A, Bowser R, Sherman M, Petrucelli L, Wolozin B (2010) Tar DNA binding protein-43 (TDP-43) associates with stress granules: analysis of cultured cells and pathological brain tissue. *PLoS ONE* 5: e13250

Ma E, MacRae IJ, Kirsch JF, Doudna JA (2008) Autoinhibition of human dicer by its internal helicase domain. *J Mol Biol* 380: 237 – 243

MacLean B, Tomazela DM, Shulman N, Chambers M, Finney GL, Frewen B, Kern R, Tabb DL, Liebler DC, MacCoss MJ (2010) Skyline: an open source document editor for creating and analyzing targeted proteomics experiments. *Bioinformatics* 26: 966 – 968

McDonald KK, Aulas A, Destroismaisons L, Pickles S, Beleac E, Camu W, Rouleau GA, Vande Velde C (2011) TAR DNA-binding protein 43 (TDP-43) regulates stress granule dynamics via differential regulation of G3BP and TIA-1. *Hum Mol Genet* 20: 1400 – 1410

Melo S, Villanueva A, Moutinho C, Davalos V, Spizzo R, Ivan C, Rossi S, Setien F, Casanovas O, Simo-Riudalbas L, Carmona J, Carrere J, Vidal A, Aytes A, Puertas S, Ropero S, Kalluri R, Croce CM, Calin GA, Esteller M (2011) Small molecule enoxacin is a cancer-specific growth inhibitor that acts by enhancing TAR RNA-binding protein 2-mediated microRNA processing. *Proc Natl Acad Sci USA* 108: 4394 – 4399

Melo CA, Melo SA (2014) MicroRNA biogenesis: dicing assay. *Methods Mol Biol* 1182: 219 – 226

Mendell JT, Olson EN (2012) MicroRNAs in stress signaling and human disease. *Cell* 148: 1172 – 1187

Meyerowitz J, Parker SJ, Vella LJ, Ng D, Price KA, Liddell JR, Caragounis A, Li QX, Masters CL, Nonaka T, Hasegawa M, Bogoyevitch MA, Kanninen KM, Crouch PJ, White AR (2011) C-Jun N-terminal kinase controls TDP-43 accumulation in stress granules induced by oxidative stress. *Mol Neurodegener* 6: 57

Milligan C, Gifondorwa D (2011) Isolation and culture of postnatal spinal motoneurons. *Methods Mol Biol* 793: 77 – 85

Mitchell JC, McGoldrick P, Vance C, Hortobagyi T, Sreedharan J, Rogelj B, Tudor EL, Smith BN, Klasen C, Miller CC, Cooper JD, Greensmith L, Shaw CE (2013) Overexpression of human wild-type FUS causes progressive motor neuron degeneration in an age- and dose-dependent fashion. *Acta Neuropathol* 125: 273 – 288

Mori MA, Raghavan P, Thomou T, Boucher J, Robida-Stubbs S, Macotela Y, Russell SJ, Kirkland JL, Blackwell TK, Kahn CR (2012) Role of microRNA processing in adipose tissue in stress defense and longevity. *Cell Metab* 16: 336 – 347

Morlando M, Dini Modigliani S, Torrelli G, Rosa A, Di Carlo V, Caffarelli E, Bozzoni I (2012) FUS stimulates microRNA biogenesis by facilitating co-transcriptional Drosha recruitment. *EMBO J* 31: 4502 – 4510

Nandal A, Ruiz JC, Subramanian P, Ghimire-Rijal S, Sinnamon RA, Stemmler TL, Bruick RK, Philpott CC (2011) Activation of the HIF prolyl hydroxylase by the iron chaperones PCBP1 and PCBP2. *Cell Metab* 14: 647 – 657

Neumann M, Igaz LM, Kwong LK, Nakashima-Yasuda H, Kolb SJ, Dreyfuss G, Kretzschmar HA, Trojanowski JQ, Lee VM (2007) Absence of heterogeneous nuclear ribonucleoproteins and survival motor neuron protein in TDP-43 positive inclusions in frontotemporal lobar degeneration. *Acta Neuropathol* 113: 543 – 548

Neumann M, Wang Y, Kim S, Hong SM, Jeng L, Bilgen M, Liu J (2009) Assessing gait impairment following experimental traumatic brain injury in mice. *J Neurosci Methods* 176: 34 – 44

Nidadavolu LS, Niedernhofer LJ, Khan SA (2013) Identification of microRNAs dysregulated in cellular senescence driven by endogenous genotoxic stress. *Aging* 5: 460 – 473

Pare JM, LaPointe P, Hobman TC (2013) Hsp90 cochaperones p23 and FKBP4 physically interact with hAgo2 and activate RNA interference-mediated silencing in mammalian cells. *Mol Biol Cell* 24: 2303 – 2310

Pelaez N, Carthew RW (2012) Biological robustness and the role of microRNAs: a network perspective. *Curr Top Dev Biol* 99: 237 – 255

Pena JT, Sohn-Lee C, Rouhanifard SH, Ludwig J, Hafner M, Mihailovic A, Lim C, Holoch D, Berninger P, Zavolan M, Tuschl T (2009) miRNA *in situ* hybridization in formaldehyde and EDC-fixed tissues. *Nat Methods* 6: 139 – 141

Peterson AC, Russell JD, Bailey DJ, Westphall MS, Coon JJ (2012) Parallel reaction monitoring for high resolution and high mass accuracy quantitative, targeted proteomics. *Mol Cell Proteomics* 11: 1475 – 1488

Qi HH, Ongusaha PP, Myllyharju J, Cheng D, Pakkanen O, Shi Y, Lee SW, Peng J, Shi Y (2008) Prolyl 4-hydroxylation regulates Argonaute 2 stability. *Nature* 455: 421 – 424

Rabin SJ, Kim JM, Baughn M, Libby RT, Kim YJ, Fan Y, La Spada A, Stone B, Ravits J (2009) Sporadic ALS has compartment-specific aberrant exon splicing and altered cell-matrix adhesion biology. *Hum Mol Genet* 19: 313 – 328

Rosen DR, Siddique T, Patterson D, Figlewicz DA, Sapp P, Hentati A, Donaldson D, Goto J, O'Regan JP, Deng HX, Rahmani Z, Krizus A, McKenna-Yasek D, Cayabyab A, Gaston SM, Berger R, Tanzi RE, Halperin JJ, Herzfeldt B, van den Bergh R *et al* (1993) Mutations in Cu/Zn superoxide dismutase gene are associated with familial amyotrophic lateral sclerosis. *Nature* 362: 59 – 62

Saxena S, Cabuy E, Caroni P (2009) A role for motoneuron subtype-selective ER stress in disease manifestations of FALS mice. *Nat Neurosci* 12: 627 – 636

Scott S, Kranz JE, Cole J, Lincecum JM, Thompson K, Kelly N, Bostrom A, Theodoss J, Al-Nakhala BM, Vieira FG, Ramasubbu J, Heywood JA (2008) Design, power, and interpretation of studies in the standard murine model of ALS. *Amyotroph Lateral Scler* 9: 4 – 15

Shan G, Li Y, Zhang J, Li W, Szulwach KE, Duan R, Faghihi MA, Khalil AM, Lu L, Paroo Z, Chan AW, Shi Z, Liu Q, Wahlestedt C, He C, Jin P (2008) A

 © 2015 The Authors

small molecule enhances RNA interference and promotes microRNA processing. *Nat Biotechnol* 26: 933 – 940

Shen J, Xia W, Khotskaya YB, Huo L, Nakanishi K, Lim SO, Du Y, Wang Y, Chang WC, Chen CH, Hsu JL, Wu Y, Lam YC, James BP, Liu X, Liu CG, Patel DJ, Hung MC (2013) EGFR modulates microRNA maturation in response to hypoxia through phosphorylation of AGO2. *Nature* 497: 383 – 387

Shi H, Bencze KZ, Stemmler TL, Philpott CC (2008) A cytosolic iron chaperone that delivers iron to ferritin. *Science* 320: 1207 – 1210

Smalheiser NR, Zhang H, Dwivedi Y (2014) Enoxacin elevates microRNA levels in rat frontal cortex and prevents learned helplessness. *Front Psychiatry* 5: 6

Sreedharan J, Blair IP, Tripathi VB, Hu X, Vance C, Rogelj B, Ackerley S, Durnall JC, Williams KL, Buratti E, Baralle F, de Belleroche J, Mitchell JD, Leigh PN, Al-Chalabi A, Miller CC, Nicholson G, Shaw CE (2008) TDP-43 mutations in familial and sporadic amyotrophic lateral sclerosis. *Science* 319: 1668 – 1672

Tahbaz N, Kolb FA, Zhang H, Jaronczyk K, Filipowicz W, Hobman TC (2004) Characterization of the interactions between mammalian PAZ PIWI domain proteins and Dicer. *EMBO Rep* 5: 189 – 194

Tortarolo M, Veglianese P, Calvaresi N, Botturi A, Rossi C, Giorgini A, Migheli A, Bendotti C (2003) Persistent activation of p38 mitogen-activated protein kinase in a mouse model of familial amyotrophic lateral sclerosis correlates with disease progression. *Mol Cell Neurosci* 23: 180 – 192

Valdez G, Heyer MP, Feng G, Sanes JR (2014) The role of muscle microRNAs in repairing the neuromuscular junction. *PLoS ONE* 9: e93140

Vance C, Rogelj B, Hortobagyi T, De Vos KJ, Nishimura AL, Sreedharan J, Hu X, Smith B, Ruddy D, Wright P, Ganesalingam J, Williams KL, Tripathi V, Al-Saraj S, Al-Chalabi A, Leigh PN, Blair IP, Nicholson G, de Belleroche J, Gallo JM *et al* (2009) Mutations in FUS, an RNA processing protein, cause familial amyotrophic lateral sclerosis type 6. *Science* 323: 1208 – 1211

Vance C, Scotter EL, Nishimura AL, Troakes C, Mitchell JC, Kathe C, Urwin H, Manser C, Miller CC, Hortobagyi T, Dragunow M, Rogelj B, Shaw CE (2013) ALS mutant FUS disrupts nuclear localization and sequesters wild-type FUS within cytoplasmic stress granules. *Hum Mol Genet* 22: 2676 – 2688

Volkening K, Leystra-Lantz C, Yang W, Jaffee H, Strong MJ (2009) Tar DNA binding protein of 43 kDa (TDP-43), 14-3-3 proteins and copper/zinc superoxide dismutase (SOD1) interact to modulate NFL mRNA stability. Implications for altered RNA processing in amyotrophic lateral sclerosis (ALS). *Brain Res* 1305: 168 – 182

Waibel S, Neumann M, Rabe M, Meyer T, Ludolph AC (2010) Novel missense and truncating mutations in FUS/TLS in familial ALS. *Neurology* 75: 815 – 817

Wegorzewska I, Bell S, Cairns NJ, Miller TM, Baloh RH (2009) TDP-43 mutant transgenic mice develop features of ALS and frontotemporal lobar degeneration. *Proc Natl Acad Sci USA* 106: 18809 – 18814

Williams AH, Valdez G, Moresi V, Qi X, McAnally J, Elliott JL, Bassel-Duby R, Sanes JR, Olson EN (2009) MicroRNA-206 delays ALS progression and promotes regeneration of neuromuscular synapses in mice. *Science* 326: 1549 – 1554

Wils H, Kleinberger G, Janssens J, Pereson S, Joris G, Cuijt I, Smits V, Ceuterick-de Groote C, Van Broeckhoven C, Kumar-Singh S (2010) TDP-43 transgenic mice develop spastic paralysis and neuronal inclusions characteristic of ALS and frontotemporal lobar degeneration. *Proc Natl Acad Sci USA* 107: 3858 – 3863

Wu C, So J, Davis-Dusenbery BN, Qi HH, Bloch DB, Shi Y, Lagna G, Hata A (2011) Hypoxia potentiates microRNA-mediated gene silencing through posttranslational modification of Argonaute2. *Mol Cell Biol* 31: 4760 – 4774

Yang YM, Gupta SK, Kim KJ, Powers BE, Cerqueira A, Wainger BJ, Ngo HD, Rosowski KA, Schein PA, Ackeifi CA, Arvanites AC, Davidow LS, Woolf CJ, Rubin LL (2013) A small molecule screen in stem-cell-derived motor neurons identifies a kinase inhibitor as a candidate therapeutic for ALS. *Cell Stem Cell* 12: 713 – 726

Zeng Y, Sankala H, Zhang X, Graves PR (2008) Phosphorylation of Argonaute 2 at serine-387 facilitates its localization to processing bodies. *Biochem J* 413: 429 – 436

Zhang Z, Almeida S, Lu Y, Nishimura AL, Peng L, Sun D, Wu B, Karydas AM, Tartaglia MC, Fong JC, Miller BL, Farese RV Jr, Moore MJ, Shaw CE, Gao FB (2013) Downregulation of microRNA-9 in iPSC-derived neurons of FTD/ALS patients with TDP-43 mutations. *PLoS ONE* 8: e76055

© 2015 The Authors